

1 **LIN28B increases neural crest cell migration and leads to transformation of trunk**
2 **sympathoadrenal precursors**

3
4 Corallo Diana^{1,*}, Donadon Michael¹, Pantile Marcella¹, Sidarovich Viktoryia², Cocchi
5 Simona², Ori Michela³, De Sarlo Miriam³, Candiani Simona⁴, Frasson Chiara⁵, Distel
6 Martin⁶, Quattrone Alessandro², Zanon Carlo⁵, Basso Giuseppe⁷, Tonini Gian Paolo¹ and
7 Aveic Sanja^{1,8,*}.

- 8
9 1. Neuroblastoma Laboratory, Fondazione Istituto di Ricerca Pediatrica Città della
10 Speranza, Padua, Italy.
11 2. Department of Cellular, Computational and Integrative Biology (CIBIO), University
12 of Trento, Italy.
13 3. Unit of Cell and Developmental Biology, Department of Biology, University of Pisa,
14 Italy.
15 4. Department of Earth, Environmental and Life Sciences (DISTAV), University of
16 Genoa, Italy.
17 5. Fondazione Istituto di Ricerca Pediatrica Città della Speranza, Padua, Italy.
18 6. Innovative Cancer Models, Children's Cancer Research Institute (CCRI), Wien,
19 Austria.
20 7. Department of Women and Child Health, Haematology-Oncology Clinic, University
21 of Padua, Italy.
22 8. Department of Dental Materials and Biomaterials Research, RWTH Aachen
23 University Hospital, Aachen, Germany.
24

25 *Correspondences: s.aveic@irpcds.org and d.corallo@irpcds.org
26

27 **RUNNING TITLE**

28 LIN28B boosts cell invasive motility.
29

30 **SOURCE DISCLOSURE**

31 This work was supported by funds from Fondazione Italiana per la Lotta al Neuroblastoma
32 and from the Fondazione Istituto di Ricerca Pediatrica Città della Speranza (project

33 number *19_07IRP*). Corallo Diana was supported by a Fondazione Veronesi (FUV)
34 Postdoctoral fellowship.

35

36 **DECLARATION OF INTEREST**

37 The authors declare no potential conflicts of interests.

38

39 **ABSTRACT**

40 The RNA-binding protein LIN28B regulates developmental timing and determines stem cell
41 identity by suppressing the *let-7* family of microRNAs. Postembryonic reactivation of
42 *LIN28B* impairs cell commitment to differentiation, prompting their transformation. In this
43 study, we assessed the extent to which ectopic *lin28b* expression modulates the
44 physiological behavior of neural crest cells (NCC) and governs their transformation in the
45 trunk region of developing embryos. We provide evidence that the overexpression of
46 *lin28b* inhibits sympathoadrenal cell differentiation and accelerates NCC migration in two
47 vertebrate models, *Xenopus laevis* and *Danio rerio*. Our results highlight the relevance of
48 *ITGA5* and *ITGA6* in the LIN28B-dependent regulation of the invasive motility of tumor
49 cells. The results also establish that *LIN28B* overexpression supports neuroblastoma
50 onset and the metastatic potential of malignant cells through *let-7a* dependent and
51 independent mechanisms.

52

53 **INTRODUCTION**

54 Neural crest cells (NCC) undergo substantial modifications in their morphology and
55 function during embryogenesis. Their highly migratory and invasive nature allows them to
56 reach distant body districts, whereas their pluripotency assures the specification of several
57 cell lineages, including peripheral neurons and the adrenal medulla [1, 2]. The initial
58 migratory wave of NCC is activated by the epithelial-to-mesenchymal transition (EMT).
59 The morphological changes triggered by EMT sustain cell migration from the neural tube,
60 invasion of the surrounding tissues, and spatial progression toward the peripheral sites
61 where cells differentiate and unfold their intrinsic features [3]. Several NCC characteristics,
62 such as motility, polarity, invasiveness, and plasticity, are largely shared by a number of
63 highly metastatic tumors, including colon [4], breast [5], oesophagus [6] and
64 neuroblastoma [7] tumors. Neuroblastoma is an embryonal malignancy responsible for

65 approximately 15% of cancer-related deaths during childhood [8]. It originates from the
66 transformed sympathoadrenal cell precursors deriving from trunk NCC [9] and is
67 characterized by vast clinical, genetic, and biological heterogeneity [10]. About half of
68 patients with neuroblastoma are stratified as high-risk (HR), having an overall survival rate
69 of less than 40% despite intensive multimodal therapy [11]. The main feature of HR
70 patients with neuroblastoma is the prevalence of metastases at disease onset. The
71 metastases to the liver, the bone marrow, the bone or lymph nodes are found in
72 approximately 50% of HR patients. Like other pediatric cancers, neuroblastoma shows a
73 low frequency of somatic mutations although alterations in several genes, including
74 *LIN28B*, have been associated with this malignancy [12].

75 The RNA binding proteins LIN28A/LIN28B were initially identified as important regulators
76 of developmental timing [13]. By inhibiting *let-7* microRNA biogenesis and through direct
77 binding of the target RNAs, LIN28 regulates numerous cellular activities that are
78 essential for embryogenesis [14], but it shows pro-tumorigenic features if maintained
79 beyond the physiologically defined timeframe [15, 16]. In neuroblastoma, the pro-
80 tumorigenic function of *LIN28B* has been attributed to either gene amplification or
81 overexpression [7]. However, the lack of experimental models in which modulated levels of
82 *LIN28B* can be studied during early developmental phases limits the possibility for a
83 comprehensive investigation of the mechanisms that sustain NCC transformation.

84 In this study, we assessed the role of the ectopically expressed zebrafish *lin28b* gene in
85 regulating trunk NCC migration and differentiation toward the sympathoadrenal lineage. In
86 two vertebrate models, zebrafish (*Danio rerio*) and *Xenopus* (*Xenopus laevis*), we
87 examined how the overexpression of *lin28b* affected the migration of trunk NCC during
88 early embryonic development. We then analyzed whether *lin28b* determined the
89 differentiation of NCC toward noradrenergic lineage. *In vivo*, a stable overexpression of the
90 human *LIN28B* gene driven by the *dβh* promoter was adopted to evaluate the probability of
91 neuroblastoma onset. In the tumor cells, we focused on evaluating the effects of the
92 prolonged overexpression of *LIN28B* on cell motility and dissemination *in vitro* and in the *in*
93 *vivo* xenograft model. Finally, we established the relevance of integrin-dependent signaling
94 in the regulation of neuroblastoma cell migration upon *LIN28B* overexpression.

95

96 **RESULTS**

97 ***Lin28b* overexpression impairs the differentiation of sympathoadrenal precursor**

98 **cells.**

99 To estimate the effects of *lin28b* overexpression during embryonic development, we
100 injected capped *lin28b* mRNA into 1-2-cell stage zebrafish embryos. We then assessed
101 the ectopic expression of the corresponding transcript and protein at different
102 developmental stages (Figure S1A) compared to the control (*ctrl*) embryos, injected with
103 either the mCherry or the GFP mRNAs (Figure S1B). Wild-type uninjected embryos were
104 used as a blank control for fluorescence screening, and as a reference sample for the
105 evaluation of Lin28b protein levels in the immunoblot assay (Figure S1B). Of note, the
106 injected fish showed no overt macroscopic phenotypes or developmental failures (Figure
107 S1C). We then verified the functionality of Lin28b by observing a significant reduction of
108 the *let-7a* expression in *lin28b* embryos (Figure S1D). To test if Lin28b affected the
109 development of sympathoadrenal neurons, we analyzed the expression of tyrosine
110 hydroxylase (*th*) and dopamine β -hydroxylase (*d β h*) as hallmarks of NCC differentiation
111 toward the sympathoadrenal lineage. The ectopic expression of *lin28b* at early stages of
112 development led to a marked reduction of both *d β h* and *th* mRNAs in the superior cervical
113 ganglia (SCG) as compared to GFP-injected controls (Figure 1A). Moreover, TH protein
114 levels also significantly decreased upon *lin28b* overexpression (Figure 1B). In addition,
115 *lin28b*-injected embryos expressed lower levels of the SCG marker *zash1a* (Figure 1C), a
116 transcription factor required for early sympathoadrenal cell specification [17]. These
117 findings imply the involvement of *lin28b* overexpression in the loss of pro-differentiating
118 signaling in sympathoadrenal cells already at early stages of embryonic development.
119 Then, to verify the evolutionary conservation of Lin28b function in the tetrapods, we
120 performed transient gain-of-function experiments on the *Xenopus* embryos. In this model,
121 it is possible to specifically target the central nervous system and NCC without affecting
122 the development of other tissues [18]. We therefore injected *lin28b* mRNA into one dorsal
123 blastomere at the four-cell stage (Figure 1D, left panel) along with GFP mRNA in order to
124 select and further analyze only embryos overexpressing *lin28b* in the developing central
125 nervous system. Comparable to the effects observed previously in the zebrafish, the
126 injected *lin28b* mRNA caused a significant reduction of the sympathoadrenal marker *reptin*
127 in the *Xenopus* embryos (Figure 1D, right panel). To assure that the observed reduction of
128 sympathoadrenal cells in *lin28b* embryos was not the result of damaged cell proliferation
129 or induced apoptosis, we stained the SCG with either EdU or activated Caspase-3/TUNEL,
130 respectively. We found no significant differences in the number of proliferating TH⁺ cells in
131 the SCG of injected embryos (Figure 1E). Similarly, Caspase-3 and TUNEL stainings
132 showed no relevant activation of apoptosis in the SCG of *lin28b* larvae (Figures 1F and

133 S2). These results confirm that *lin28b* overexpression determines the failure of
134 sympathoadrenal progenitor cell differentiation toward their functional counterparts without
135 affecting their proliferation or viability.

136

137 **Impaired cell differentiation promotes neuroblastomagenesis in *LIN28B*-** 138 **overexpressing zebrafish.**

139 To assess whether the *lin28b*-dependent block of peripheral sympathetic neural cell
140 differentiation has pro-tumorigenic effects in fish, we generated the stable transgenic
141 zebrafish line *Tg(dβh: hLIN28B)*, referred to here as *hLIN28B*. For this purpose, *hLIN28B*
142 was overexpressed in the peripheral sympathetic nervous system under the control of the
143 *dβh* promoter. Tumor masses arose in the anterior abdomen of six-month-old transgenic
144 animals (Figure 2A) with a 2.4% penetrance. The tumors were found in the interrenal
145 gland (IRG), a common site of neuroblastoma onset [19], and consisted of small,
146 undifferentiated, round tumor cells with distinct single nucleoli (Figure 2B). To molecularly
147 characterize and assure the tumor type, we analyzed the expression of several
148 neuroblastoma-specific markers. The tumor cells were strongly immunoreactive for TH
149 (Figure 2C), indicating their peripheral sympathetic neuronal origin [20]. They were also
150 positive for the HuC/D and the Synaptophysin markers (Figure 2C), demonstrating that
151 they arose from sympathetic neuroblast precursors, like human neuroblastomas, and not
152 from other NCC-derivatives, such as chromaffin cells. Together, these findings evince that
153 the overexpression of *hLIN28B* in the peripheral sympathetic neuronal system of
154 transgenic fish promotes neuroblastomagenesis with a penetrance below 5%,
155 approximately as described for human patients with neuroblastoma.

156 **Overexpressed *lin28b* increases the migratory capacity of trunk NCC**

157 The different number of sympathoadrenal cells composing the SCG between the *lin28b*
158 and control fish reflects the possible involvement of mechanisms regulating either NCC
159 migration or their specification during the early phases of functional commitment. To
160 assess this hypothesis, we used the *Tg(sox10:GFP)* zebrafish transgenic line [21]. In
161 these fish, GFP expression is regulated by the NCC promoter *sox10*, allowing the real-time
162 tracking of the NCC inside developing embryos. Transient overexpression of *lin28b*
163 influenced the migration of trunk NCC, as confirmed by live cell imaging, without
164 influencing the total number of GFP⁺ cells (Figure S3A), their proliferation and viability
165 (Figures S3B and S3C). Interestingly, although NCC from both the control and *lin28b*

166 embryos migrated ventrally along somites in narrow stripes as expected (Figure 3A;
167 Supplemental Video S1A), the NCC overexpressing *lin28b* were first to reach their
168 destination toward the dorsal aorta (Figure 3A; Supplemental Video S1B). To quantify this
169 phenomenon, we measured the migration distances of NCC labeled with *crestin* riboprobe
170 (Figure 3B) [22]. The average NCC migration distance was significantly longer in *lin28b*
171 embryos compared to the controls at both monitored time points (Figure 3C). Importantly,
172 the same behavior was also evident in the *Xenopus* embryos, where *lin28b*-
173 overexpressing *sox10*⁺ NCC cells [23] reached longer distances in the *lin28b* versus the
174 control side of the embryo within the same timeframe (figure 3D). Together, these data
175 prove that Lin28b regulates the migration of trunk NCC in different vertebrate models
176 without affecting their proliferation and survival rates. Following, to test how effective
177 Lin28b was in determining the sympathoadrenal lineage specification, we assessed the
178 capability of NCC to form cell lineages other than the sympathoadrenal lineage. First, we
179 analyzed the development of melanocytes originating from trunk NCC [24]. The amount of
180 melanocytes in the yolk sac and the yolk extension was unaffected upon *lin28b*
181 overexpression (Figure 3E). Moreover, a comparable number of sensory neurons
182 composing the trunk NCC-derived dorsal root ganglia (DRG) was found in both control and
183 *lin28b* larvae (Figure 3F). Furthermore, the DRG developed in the middle of the single
184 somite boundary, as expected [25]. We then looked at the enteric neurons deriving from
185 vagal NCC [26]. Upon staining with the anti-HuC/D antibody, no significant differences in
186 the number of enteric neurons were found between the control and *lin28b* larvae (Figure
187 3G). The finding that *lin28b* embryos lacked trunk NCC-derived sympathoadrenal
188 precursor cells but maintained vagal NCC-derived neurons indicates that Lin28b may play
189 different roles in the designation of specific sub-populations of trunk NCC.

190 **Overexpression of *LIN28B* increases the migratory capacity of SH-SY5Y cells**

191 To functionally test the observed *in vivo* correlations between *lin28b* overexpression and
192 the increased NCC migratory phenotype, we overexpressed *LIN28B* in the neuroblastoma
193 cell line SH-SY5Y under a short-term (48 hours) and a long-term (7 days and 14 days)
194 period. *LIN28* is known to be a master regulator of pluripotency in embryonic stem cells
195 [23, 27]. Gene expression analysis indicated that 48 hours of *LIN28B* overexpression
196 significantly increased the levels of the stemness-associated genes *Oct4*, *Sox2*, and
197 *Nestin* (Figure 4A) while preserving colony formation and cell proliferation potentials upon
198 long-term expression of *LIN28B* in SH-SY5Y cells (SH-SY5Y^{LIN28B}) and the controls (SH-
199 SY5Y^{CTRL}) (Figures S4A and S4B). Importantly, while *LIN28B* and *let-7a* expression

200 patterns showed reciprocal expressions after short-term *LIN28B* induction, the *let-7a* levels
201 reverted after prolonged overexpression (Figure 4B). These findings imply that intervals of
202 *LIN28B* overexpression define molecular mechanisms that can be both *let-7a*-dependent
203 and *let-7a*-independent. Long-term *LIN28B* overexpression provoked consistent changes
204 in cell morphology (Figures 4C and S4C), which was accompanied by a notable
205 reorganization of cytoskeleton microfilaments (Figures 4D and S4D). Indeed, SH-
206 SY5Y^{CTRL} cells formed small and stellate-shaped cell clumps, whereas SH-SY5Y^{LIN28B}
207 cells were bigger and cuboidal in shape. Given the role of cytoskeleton reorganization in
208 cell motility [28] and the observed higher migratory rates of NCC upon *lin28b*
209 overexpression *in vivo*, we analyzed the correlation between these phenomena *in vitro*.
210 Ectopic *LIN28B* significantly increased the migratory properties of SH-SY5Y^{LIN28B} cells, as
211 revealed by scratch and transwell assays (Figure 4E, F). A detailed analysis of cell
212 movement using time-lapse imaging showed a sharp increase in total migrated distances
213 (Figures 4G and S4E, Supplemental Movies S2A and S2B) and in the mean cell velocities
214 of SH-SY5Y^{LIN28B} cells upon 7 days of *LIN28B* induction (Figure 4H). Notably, motility
215 continued to progress upon *LIN28B* induction for 14 days (Figures S4F-H, Supplemental
216 Movies S3A and S3B). These results provide further evidence that *LIN28B* overexpression
217 is a determinant factor for defining the migration of neural crest-derived cells both *in vitro*
218 and *in vivo*.

219

220 **LIN28B promotes the invasive motility of neuroblastoma cells**

221 The core feature of highly aggressive tumors is their metastatic potential determined by
222 enhanced cell migration and invasion abilities. Both features are also mandatory for the
223 proper function of NCC during embryogenesis. To investigate whether *LIN28B* may
224 sustain cell invasiveness, we analyzed the capacity of SH-SY5Y^{LIN28B} cells to infiltrate the
225 matrigel-coated Boyden chambers (Figure 5A, upper panel). This assay confirmed an
226 increased capacity of SH-SY5Y^{LIN28B} cells to invade the basement membrane following a
227 chemo-attractant gradient when compared to the control SH-SY5Y^{CTRL} counterpart (Figure
228 5A, graph bars). To confirm these findings *in vivo*, we injected either SH-SY5Y^{LIN28B} or SH-
229 SY5Y^{CTRL} cells into the duct of Cuvier of *Tg(fli1:GFP)* zebrafish embryos with blood
230 vessels marked in green. While SH-SY5Y^{LIN28B} cells showed a rapid spread inside the
231 vessels and clear distribution throughout the trunk of the embryos one-day post injection,
232 SH-SY5Y^{CTRL} cells did not disseminate in the same way (Figure 5B). This pro-invasive
233 phenotype was sustained by EMT induction, as SH-SY5Y^{LIN28B} cells expressed

234 significantly higher levels of the mesenchymal markers N-cadherin, Snail, Twist1, and Slug
235 compared to the control cells upon long-term *LIN28B* induction (Figures 5C and S5A).
236 Consistently, the levels of *N-cadherin*, *Snail*, *Twist1*, and *Slug* genes were also
237 significantly upregulated after *LIN28B* ectopic expression (Figure 5D). These findings
238 explained the previously observed changes in SH-SY5Y^{LIN28B} cell morphology (Figure 4D)
239 that aligned well with the mesenchymal-like phenotype. In line with these outcomes, the
240 overexpression of *lin28b* in the zebrafish embryos led to a global activation of EMT
241 (Figures 5E, 5F, and 5G) as well. Taken together, the results imply that LIN28B is
242 sufficient to trigger EMT and to increase the invasive capacities of neural crest-derived
243 neuroblastoma cells.

244

245 **LIN28B activates integrin-signaling pathways**

246 The migration of trunk NCC during body segmentation and somitogenesis is mediated by
247 their interaction with the extracellular matrix (ECM) components. Integrins are a family of
248 transmembrane receptors required for cell adhesion and their migration [29-31]. To
249 investigate whether the acquired migratory and invasive potentials of *LIN28B*-
250 overexpressing neuroblastoma cells could be attributed to integrin signaling, we evaluated
251 the gene expression patterns of a number of integrins. Out of the nine transcripts
252 analyzed, the most apparent upregulation was found for two integrins, α5-integrin (*ITGA5*)
253 and α6-integrin (*ITGA6*). Both of these showed a substantial induction upon prolonged
254 *LIN28B* overexpression (Figure 6A). Accordingly, the expression of the corresponding
255 proteins, ITGA5 (CD49e) and ITGA6 (CD49f), was triggered in SH-SY5Y^{LIN28B} cells
256 (Figures 6B and S5B-D) and confirmed by flow cytometry analyses (Figures 6C and 6D).
257 Then, to assess the importance of the two transmembrane proteins in the regulation of
258 SH-SY5Y^{LIN28B} cell motility, we examined their migration upon the addition of antagonizing
259 primary antibodies. Pre-treatment with either the blocking antibodies anti-ITGA5
260 (ITGA5ab) or anti-ITGA6 (ITGA6ab) successfully abolished the migration of *LIN28B*-
261 overexpressing cells (Figures 6E and 6F, Supplementary Videos S5-S8). Correspondingly,
262 cell speed was dramatically reduced only in ITGA5ab- and ITGA6ab-treated SH-
263 SY5Y^{LIN28B} cells, suggesting that the previously described pro-migratory phenotypes were
264 largely hooked up by the two cell-surface integrins in *LIN28B*-overexpressing cells.
265 Because the integrin clustering is essential for the early phases of cell adhesion to the
266 substrate, we next assessed if the observed phenotype was associated with altered focal
267 adhesions' (FAs) formation. While the SH-SY5Y^{CTRL} cells exhibited a diffuse cytosolic

268 distribution of FA adaptor proteins Paxillin, focal adhesion kinase (FAK), and Vinculin [32],
269 the SH-SY5Y^{LIN28B} cells possessed these proteins organized on the plasma membrane as
270 punctate, peripheral adhesions (Figures 7A and S6A). At day 7, these modifications were
271 sustained mainly by the activation of two integrin/FAK-related signaling routes, including
272 PI3K p85/AKT^{Ser473} and Src pathways (Figures 7B and S6B). Both signaling cascades are
273 important players in regulating the integrin-based cell motility [33]. However, at day 14 only
274 ERK activation was detected (Figure S6C), implying for a dynamic temporal regulatory
275 switch between multiple signaling proteins in *LIN28B*-overexpressing cells. Taken
276 together, our observations attribute to LIN28B a novel role in orchestrating the integrin-
277 mediated cell spreading and migration.

278

279 **DISCUSSION**

280 The highly conserved RNA-binding protein LIN28B is expressed in developing tissues and
281 is required for proper embryogenesis [13]. One of the most recognized roles of LIN28B
282 involves the inhibition of the tumor suppressing *let-7* family of microRNAs [14], contributing
283 to the maintenance of cell pluripotency. The altered expression of *LIN28B* has been
284 reported in various types of human cancer [4, 35, 36] while its role as an oncogene has
285 been confirmed in different mouse models [7, 37]. In neuroblastoma, genomic amplification
286 or overexpression of *LIN28B* are associated with the HR group of patients for whom the
287 widespread metastatic disease is regularly present [7]. Nevertheless, *LIN28B*-driven
288 mechanisms of tumorigenesis are still poorly characterized for neuroblastoma, especially
289 because the onset of this tumor occurs during the early embryonic developmental stages.

290 In this study, we assessed the *in vivo* effects of fish *lin28b* overexpression on the NCC
291 compartment. We relied on the zebrafish and *Xenopus* vertebrate models to demonstrate
292 that the ectopic expression of *lin28b* led to a block in the differentiation of NCC-derived
293 sympathetic progenitor cells without affecting their proliferation or vitality. We showed that
294 Lin28b is required for the commitment of trunk NCC toward the sympathoadrenal cell
295 lineage but is dispensable for the delineation of other NCC derivatives, such as pigmented
296 cells and enteric neurons. This raises the possibility that Lin28b-derived signaling may act
297 in specific NCC sub-populations in which the overexpression of *lin28b* beyond its
298 physiological timeframe is sufficient for the malignant transformation of trunk
299 sympathoadrenal cell precursors and for neuroblastoma's onset. In fact, the transgenic
300 zebrafish model with *dβh*-driven overexpression of *hLIN28B* caused tumors in six-month-
301 old fish. These tumors showed high immunohistochemical similarities with human

302 neuroblastomas and with previously reported neuroblastomas developed in zebrafish [38].
303 More importantly, the penetrance of LIN28B-positive tumors in fish aligned to the one
304 previously described for human neuroblastomas. We then studied the molecular
305 consequences of enforced short-term and long-term overexpression of the *LIN28B* gene *in*
306 *vitro* in NCC-derived neuroblastoma cells. We could distinguish the short-term and long-
307 term effects of *LIN28B* overexpression as respectively *let-7a*-dependent and *let-7a*-
308 independent, sustaining previous findings [39]. Moreover, the LIN28B-driven acquisition of
309 migratory and invasive properties was accompanied by substantial morphological changes
310 and the increase of several mesenchymal markers, sustaining *LIN28B* as a promoter of
311 EMT. During normal embryonic development, NCC undergo EMT and the subsequent
312 migration is largely dependent on the cell-ECM crosstalk. Integrins are composed of
313 diverse heterodimeric transmembrane receptors transducing the signals bidirectionally and
314 regulating cell adhesion, migration, and invasion [40]. In our study, we identified a
315 significant increase of two integrins, ITGA5 and ITGA6, upon long-term *LIN28B*
316 overexpression. The importance of ITGA6 in inducing metastasis has been reported in
317 several cancer types diagnosed in adults [41, 42], whereas in neuroblastoma, its
318 involvement in cell dissemination was not previously described. Conversely, ITGA5
319 induction has been recently associated with a metastatic neuroblastoma phenotype [43].
320 Consistent with previous findings, our results highlight the importance of integrin-mediated
321 pro-metastatic behavior in *LIN28B*-overexpressing neuroblastoma cells. They also sustain
322 the role of LIN28B in facilitating a dynamic remodeling of cell adhesion proteins [44]. The
323 recruitment of FA clusters on the plasma membrane of *LIN28B*-overexpressing cells
324 implies their value for sustaining the migratory properties of tumor cells. In this scenario,
325 the activation of downstream pathways at first involved the PI3K/AKT and Src kinases,
326 followed by a delayed ERK engagement. All of them were described along with a shift
327 toward more motile phenotypes and a favored FA formation [45]. These results imply that
328 *LIN28B* overexpression promotes mesenchymal-like phenotypes whose motility is allowed
329 by the Integrin/FAK axis and dynamic regulation of several intracellular pathways.
330 Moreover, the striking expression of ITGA5/ITGA6 on the SH-SY5Y^{LIN28B} cell membrane
331 may be critical for shaping the interaction between the ECM and tumor cells and, hence,
332 for their motility and invasion capacities. Both characteristics are required for tumor cells'
333 dissemination and metastasis formation. Our findings specify additional roles of LIN28B in
334 the regulation of the interaction between neuroblastoma cells and their surrounding niche.
335 Previous reports affirm the abundance of fibronectin and laminin, high-affinity binding
336 targets of ITGA5 and ITGA6, within the trunk region of the zebrafish embryos [46, 47].

337 Their neutralization provokes the inhibition of NCC migration, pointing out the relevance of
338 both ECM molecules for the proper function of NCC [47]. Hence, *hLIN28B*-overexpressing
339 zebrafish could allow not only novel understandings of the cell-ECM interactions but may
340 also serve as an *in vivo* model for evaluating the effects of selective integrin inhibitors in
341 the treatment of metastatic neuroblastoma.

342 In conclusion, we confirmed the oncogenic potential of *LIN28B* and its association with
343 neuroblastoma's onset in the zebrafish model. We showed a positive correlation between
344 *LIN28B* overexpression and the induction of EMT, a process that led to the cell
345 morphology transformation and increment of invasive traits of tumor cells. We additionally
346 highlighted the complexity of the *LIN28B*-dependent pathways not necessarily involving
347 *let-7a* miRNA. Further, we described the association between *LIN28B* overexpression and
348 the pro-metastatic phenotype of neuroblastoma cells. This feature was triggered by
349 activating *ITGA5* and *ITGA6* expression and by the accumulation of corresponding
350 proteins on the cell membrane. Together, our results suggest that *LIN28B* sustains
351 integrin-mediated cell spreading and migration by facilitating the formation of focal
352 contacts. The two integrins, *ITGA5* and *ITGA6*, could therefore be new molecular markers
353 in pro-metastatic neuroblastoma. Further investigation on whether they might be potential
354 targets in a group of HR patients remains to be performed.

355

356 **MATERIALS AND METHODS**

357 **Animals.** Wild-type (AB/TU) zebrafish [48] and the transgenic line *Tg(sox10:GFP)* [21]
358 were staged and maintained as described previously [49]. All experiments using animal
359 models were approved by the local Ethical Committees and by the Italian Ministry of
360 Health (zebrafish authorization 86/2016-PR; *Xenopus* authorization 99/2012-A). *Xenopus*
361 embryos were obtained and staged as described previously [17].

362 **Cell lines.** SH-SY5Y cells were purchased from the DSMZ (Germany) and grown in RPMI-
363 1640 (Sigma-Aldrich) with the addition of 2 mM penicillin/streptomycin (Gibco), 2mM L-
364 glutamine (Gibco), and 10% fetal bovine serum (FBS; Gibco). Cell line genotyping was
365 conducted prior to the analyses.

366 SH-SY5Y^{CTRL} and doxycycline-inducible SH-SY5Y^{LIN28B} cell lines were obtained by a
367 lentiviral infection; pLenti CMV CTRL Blast plasmid (Addgene #17492) and modified pLenti
368 CMV/TO GFP Puro plasmid (GFP was replaced by *LIN28B* ORF, Addgene, #17481) were
369 used. Lentiviral particles were produced by co-transfecting either the CTRL or *LIN28B*

370 plasmids with the packaging vector psPAX2 (Addgene #12260) and the envelope plasmid
371 pMD2.G (Addgene #12259) into HEK-293T cells (ICLC) in the Opti-MEM culture medium
372 (Gibco) with 1 mg/ml polyethylenimine (Sigma-Aldrich). The cells stably expressing the
373 TetR control gene (SH-SY5Y^{CTRL}) were grown in 7 µg/ml of Blasticidin-S HCl (Gibco)
374 enriched selecting medium. A population of SH-SY5Y^{LIN28B} cells was generated upon
375 growth in 2 µg/ml of puromycin (Gibco) enriched selective medium.

376 **Capped mRNA overexpression.** The SP6 Message machine kit (Ambion) was used to
377 transcribe synthetic capped RNA. Zebrafish embryos were injected with 50-100 pg of
378 *lin28b* or *GFP* mRNA at the one-two-cell stage. Injected embryos were raised from 16
379 hours post fertilization (hpf) to 6 days post fertilization (dpf) and fixed with 4%
380 paraformaldehyde for further analysis. Xenopus embryos were injected with *lin28b* or *GFP*
381 mRNA in one blastomere at the four-cells stage and then fixed with 4% paraformaldehyde
382 for further analysis.

383 **Constructs and probes.** The pCS2⁺-mCherry construct was a kind gift of Dr. Enrico Moro
384 (University of Padua). The pCS2⁺-GFP was generated from the pME-GFP construct from
385 the Multisite Gateway-based construction kit (To2Kit) [50]. Zebrafish *lin28b* cDNAs were
386 obtained by PCR and cloned into the pCS2⁺ vector. The pcDNA3-FLAG-*LIN28B* construct
387 used for the doxycycline-inducible SH-SY5Y cell line was a kind gift from Narry Kim
388 (Addgene plasmid #51373). The following antisense RNA probes were also generous gifts:
389 *dbh*, *th* [51], and *zash-1a* [52]. The *crestin* probe was generated by amplifying
390 the zebrafish ORF from the wild-type whole embryo cDNA, and the PCR product was
391 cloned into the pCR-II-TOPO vector (Invitrogen). Following sequence verification,
392 antisense riboprobes were generated by *in vitro* transcription with a DIG RNA labeling kit
393 Sp6/T7 (Roche). Antisense riboprobes were also generated following sequence
394 verification through *in vitro* transcription with a DIG RNA labeling kit Sp6/T7 (Roche). The
395 *dre-let-7a* probe was purchased from EXIQON. The Xenopus pCS2⁺-*lin28b* plasmid was
396 generated by RT-PCR and fully sequenced. The plasmids used for the preparation of
397 *reptin* and *sox10* antisense RNA probes are described elsewhere [53, 54].

398 **Transgenesis.** The 5.2-kb promoter region of the *dβh* gene was PCR amplified from the
399 zebrafish BAC clone CH211-270H11 (<https://bacpacresources.org/>) using the primers dβh-
400 fw (#599): GCG TAC TCC CCC TTT TTA GG and dβh-rev (#600): TGT TGC TTT GTC
401 GTC TTT TGA. The PCR product was cloned into the gateway p5-MCS vector (a kind gift
402 of the Chien lab) using the KpnI/XhoI restriction sites. *LIN28B* was isolated from pcDNA3-
403 Flag-*LIN28B* (Addgene #51373) by BamHI/NotI digestion and cloned into the gateway

404 middle entry vector pENTR1A using the same restriction enzymes. The full transgenesis
405 construct was gateway assembled [50] to generate the pDEST5.2*dβh-LIN28B*-CG2. The
406 embryos were injected with this DNA construct at the one-cell stage and grown to
407 adulthood. Fin clips from the offspring were used for the genotyping of stable integration
408 and the germline transmission of the transgene. The *Tg(dβh: hLIN28B)* was designated as
409 the '*hLIN28B*' transgenic line in this article.

410 ***In situ* hybridization.** Whole-mount RNA *in situ* hybridization (WISH) of zebrafish and
411 *Xenopus* embryos was performed, as previously described [55, 17]. Briefly, fixed embryos
412 were permeabilized with 10 μg/ml of Proteinase K and, after five hours of pre-incubation
413 with Hybridization Mix (50% Formamide, 5X SSC, 0.01% Tween-20, 50 μg/ml of heparin,
414 500 μg/ml of t-RNA), they were incubated with 100 ng/μl of the antisense probe at 65° C.
415 The second day, embryos were extensively washed and incubated in a Blocking Solution
416 (2% sheep serum, 2 mg/ml of BSA in PBS/0.1% Tween-20) for two hours, followed by the
417 addition of the Anti-Digoxigenin antibody (Anti-Digoxigenin-AP Fab fragment, Roche),
418 diluted 1:3000. The embryos were washed several times in PBTw, followed by the
419 incubation with the Staining Solution containing NBT/BCIP (Roche). Stained embryos were
420 sectioned and mounted in 80% glycerol, and images were acquired with a Carl Zeiss Axio
421 microscope.

422 **Immunofluorescence.** Immunofluorescence of whole zebrafish embryos was performed
423 essentially as described [56]. Fixed embryos were permeabilized in cold acetone for seven
424 minutes at -20° C, followed by three washes in PBTx (1% Triton X-100 in 1X PBS) for five
425 minutes at RT in agitation. The embryos were blocked in 3% goat serum diluted in PBTx
426 for one hour in agitation, and primary antibodies were then added overnight at 4° C. The
427 embryos were washed three times in PBTx for 10 minutes and incubated with secondary
428 antibodies in 5% goat serum/PBTx in the dark for three hours. Lastly, the embryos were
429 washed two times in PBTx for 10 minutes and transferred in low melting 1.5% agarose
430 (Sigma-Aldrich) and mounted in slides, and images were acquired with a Carl Zeiss Axio
431 microscope and a Leica TCS-SP5-II confocal microscope. Primary and secondary
432 antibodies are listed in Supplemental Table S1.

433 SH-SY5Y cells were fixed using 4% PFA in PBS for 15 minutes before permeabilization
434 with 0.1% Triton X-100 diluted in PBS. To reduce the background fluorescence, the
435 coverslips were blocked in 3% BSA prepared in PBS for one hour at room temperature.
436 Cells were stained with phalloidin-TRITC, ITGA5, and ITGA6 antibodies. The cells in
437 Figures S5C and S5C were incubated with 3% BSA without cell permeabilization. The

438 proteins were visualized with a Zeiss LSM 800 confocal microscope. For Paxillin, FAK, and
439 Vinculin staining, the coverslips were fixed and permeabilized as previously described.
440 The coverslips were subsequently treated with primary antibodies for one hour and after
441 PBS washing with a secondary antibody in a dark humid chamber for 45 minutes. The
442 coverslips were subsequently mounted on glass slides and observed by confocal
443 microscopy (Zeiss LSM 800 confocal microscope). The number of FAs per cell was
444 assessed using ImageJ software.

445 **Western blot.** Zebrafish-derived proteins were extracted from pools of 30 embryos
446 through mechanical desegregation in Lysis Buffer (Tissue Extraction Reagent I, Life
447 Technologies) supplemented with 1% Protease/Phosphatase Inhibitor Cocktail (Sigma
448 Aldrich). The proteins from neuroblastoma cells were extracted with commercially
449 available lysis buffer (Biosource International) from the samples pre-treated with
450 doxycycline, as described previously [57].

451 Samples were centrifuged at 14,000 g for five minutes at 4° C, and the protein
452 concentration was determined using the bicinchoninic assay (BCA) method (Pierce BCA
453 Protein Assay Kit, Thermo Scientific). A total amount of 50 µg (zebrafish) and 20 µg (cell
454 lines) of proteins were loaded in the Criterion™ TGX Stain-Free™ Precast Gels 4-20%
455 (Bio-Rad) and then transferred on the nitrocellulose membrane (Midi-size LF PVDF
456 Membrane, TransBlot® Turbo™, Bio-Rad, activated in 100% Methanol) through a semi-dry
457 transfer with the Trans-Blot® Turbo™ Transfer System (Bio-Rad). Membranes were
458 blocked with Tropix® I-BLOCK (Thermo Fisher Scientific) for two hours, followed by
459 incubation with primary antibodies at 4° C. The membranes were washed and incubated
460 with secondary antibodies. Uvitec Cambridge was used for chemiluminescence detection,
461 covering the membrane with ECL (ECL Select™ Western Blotting Detection Reagent, GE
462 Healthcare). The primary and secondary antibodies are listed in Supplemental Table S1.

463 **EdU proliferation and TUNEL cell death assays.** A proliferation assay was performed
464 using a commercial kit, EdU-Click 488, as recommended by the manufacturer (Baseclick).
465 Briefly, three independent pools of 15 living embryos were collected in microcentrifuge
466 tubes, and 1 mM EdU was added, followed by incubation on ice for a variable time
467 depending on their developmental stage. The embryos were washed with cold E3 medium
468 on ice and then incubated for 30 minutes at 28.5° C. After that, embryos were fixed with
469 4% paraformaldehyde for two hours and permeabilized in 10 µg/ml Proteinase K. To
470 detect proliferating cells, embryos were incubated in the Reaction Cocktail containing 10
471 mM of Dye Azide for three hours. In following, the embryos were used for the coupled

472 immunostainings to detect the SCG or the NCC. Cell death assay was performed using a
473 commercial kit, Click-iT Plus TUNEL Assay, following manufacturer instruction (Life
474 Technologies). Fixed embryos were permeabilized with 10 µg/ml Proteinase K and
475 subsequently incubated with an Equilibration Buffer (TdT reaction buffer) for one hour.
476 Next, the embryos were incubated with the TdT enzyme for 90 minutes at 37° C and then
477 with the Reaction Cocktail for 30 minutes at 37° C. The embryos were fixed again in 4%
478 paraformaldehyde for 30 minutes, and the immunofluorescence with the anti-GFP antibody
479 was then performed (see Supplemental Table S1). The embryos were then mounted in 3%
480 methylcellulose, and images were acquired through a Zeiss LSM 800 confocal
481 microscope.

482 **Fluorescent cell labeling, embryo preparation, and tumor cell implantation.** After
483 seven days of doxycyclin administration, SH-SY5Y^{CTRL} and SH-SY5Y^{LIN28B} cells were
484 labeled with the Vybrant® Dil Cell-Labeling Solution (Invitrogen) according to the
485 manufacturer's instructions. The dechorionized (2 dpf) zebrafish embryos were
486 anaesthetized with 0.003% tricaine (Sigma-Aldrich) and positioned on a 10 cm Petri dish
487 coated with 3% agarose. Approximately 200 cells were injected within the duct of Cuvier of
488 the anesthetized *Tg(fli1:GFP)* embryos using borosilicate glass capillary needles (OD/ID:
489 1.0/0.75 mm, WPI), a Pneumatic Picopump, and a micro-manipulator (WPI). After
490 implantation, zebrafish embryos were maintained at 33° C. Embryos showing less than 30-
491 40 cells after four hours post-injection were discarded from the analysis. At least 50
492 embryos per group were analyzed from three independent experiments. The embryos
493 were live photographed using a Nikon C2 H600L confocal microscope (20X water dipping
494 objective).

495 **Time-lapse.** *Tg(sox10:GFP)* embryos were injected with *LIN28B* mRNA and allowed to
496 develop for 19-20 hpf. Anesthetized embryos were embedded in 1.5% agar, mounted in a
497 heated chamber, and imaged with a Zeiss Axio Observer microscope for live cell imaging
498 for eight hours. Quantification of displacement was measured in a 40 µm Z-stack, tracked
499 using Fiji software. The quantification of the percentage of the migrated distance relative to
500 Figure 3B was the measurement of the straight-line distance from the first position (neural
501 tube) to the last position labeled with *crestin* riboprobe, with a higher number indicative of
502 more distance between the first and last point. Statistical analysis was conducted in Excel
503 followed by a two-tailed Student's t-test. Neuroblastoma cells were analyzed in a 37° C
504 heated chamber with 5% CO₂. Cell motility was captured over a 12-hour period at 10
505 minute intervals, and tracks were recorded using the Fiji "manual tracking" plug-in. For

506 functional integrin blocking, the attached cells were pre-incubated for 30 minutes before
507 migration analysis either with 10 µg/ml of mouse anti-human-ITGA6 or mouse anti-human-
508 ITGA5 antibodies in 24 well plates (see Supplemental Table S1). The appropriate IgG
509 antibodies (Mouse IgG2b, Millipore; Mouse IgG1, Santa Cruz Biotechnology) were used as
510 negative controls. Cell motility was captured over a 12-hour period at 10-minute intervals.

511 The Wilcoxon test was used to assess the p-values quantifying the significance of the
512 differences. All statistical analyses were performed using the R statistical software 'stats'
513 package.

514 **Flow cytometric analyses.** Zebrafish single-NCC were obtained from the pool of 40
515 embryos. *Tg(sox10:GFP)* and wild-type zebrafish embryos were dissected to remove the
516 head and washed, and the tails were mechanically desegregated by constant pipetting in
517 Hanks' buffer (EMD Millipore Corporation). Single-NCC were obtained using Trypsin-
518 EDTA (EMD Millipore Corporation) and Collagenase/Dispase (Sigma-Aldrich). After
519 resuspending the NCC in Hanks' buffer, analyses were performed through Cytomics FC
520 500 (Beckman Coulter). Wild-type uninjected embryos were used as blanks.

521 SH-SY5Y^{CTRL} and SH-SY5Y^{LIN28B} cells (0.3-0.5 x 10⁶ cells) were incubated with PeCy5
522 anti-human CD49f (ITGA6, Becton Dickinson) and analyzed using a CytoFLEX Flow
523 cytometer (Beckman Coulter). The percentage of CD49e (ITGA5) positive cells was
524 validated upon coupled primary (1 µg) and secondary antibody labeling (see Supplemental
525 Table S1). The percentage of CD49e- and CD49f-positive cells in both SH-SY5Y^{CTRL} and
526 SH-SY5Y^{LIN28B} cells were considered by setting an appropriate gate on the living cell
527 population (Propidium iodide negative, 10 mg/ml, Roche). Unlabeled cells for each line
528 were first acquired to ensure labeling specificity.

529 **Colony formation assay.** Two thousand cells were seeded in a 24-well plate using a
530 MethoCult semi-solid medium (Stemcell Technologies) and were grown for two weeks.
531 Colonies (foci) were visualized after incubation with MTT. The total colony number was
532 counted under a light microscope in ten random fields and determined by Fiji software.

533 **Transwell migration assay.** SH-SY5Y^{CTRL} and SH-SY5Y^{LIN28B} cells were seeded onto
534 inserts without Matrigel (BD Biosciences) in a serum-free medium. Inserts were placed into
535 wells containing a medium supplemented with 10% FBS. After 24 hours, the cells on the
536 upper surface of the filters were removed, and the inserts were stained with Hoechst
537 (Sigma-Aldrich) and cristalviolet. The numbers of migrated cells were counted under a light

538 and a fluorescent microscope in ten random fields. Using Fiji software, the number of
539 migrated cells per image was determined.

540 **Matrigel invasion assay.** SH-SY5Y^{CTRL} and SH-SY5Y^{LIN28B} cells (5×10^4) were seeded
541 onto matrigel-coated transwell chambers (BD Biosciences) with an 8- μ m pore size filter
542 using an FBS gradient (0-10%) from the top to the bottom well. After 24 hours of
543 incubation, the filter was removed and washed, and the cells that invaded the lower side of
544 the filter were stained with calcein (Sigma-Aldrich). The absorbance was measured using
545 the VICTOR™ Multilabel Plate Reader (PerkinElmer, Waltham, MA) at 495 nm.

546 **Scratch test.** SH-SY5Y^{CTRL} and SH-SY5Y^{LIN28B} cells (3×10^4) were plated within each of
547 the two-cell culture reservoirs separated by a 500- μ m-thick silicone wall (IBIDI, Milano,
548 Italy). The day after, the silicone insert was removed and the cells were allowed to grow for
549 another 48-72 hours. Images were taken every 24 hours by a Nikon Eclipse TS100
550 microscope (Nikon Eclipse TS 100, Southern Micro Instruments, Marietta, GA) equipped
551 with a Nikon Coolpix camera. Wound healing was analyzed by Fiji software for each time
552 point.

553 **RNA analysis.** Total RNA was extracted from the pool of 30 embryos or cell pellets using
554 TRIzol Reagent (Invitrogen), and 2 μ g of RNA were used for cDNA synthesis using Super
555 Script II (Invitrogen), according to the manufacturer's recommendations. The cDNA was
556 subjected to PCR reaction using the AmpliTaq DNA polymerase (Thermo Fisher
557 Scientific).

558 The expression of *lin28b*, *cdh1*, *snail1a*, *twist1a*, and vimentin transcripts was analyzed by
559 real-time quantitative PCR (qPCR) using the SYBR Green PCR Master Mix (Applied
560 Biosystems) in an Applied Biosystems 7900HT Fast Real Time PCR System. Primer
561 dissociation curves were checked in each run to ensure primer specificity in human and
562 zebrafish mRNA. The expression of *gapdh* was used as a normalizer in each sample, and
563 triplicate PCR reactions were carried out. Primers were designed using the Primer 3
564 software (<http://bioinfo.ut.ee/primer3-0.4.0/input.htm>) and are listed in Supplemental Table
565 S2.

566 **MicroRNA (miRNA) measurement by qPCR.** Total RNA was isolated from SH-SY5Y^{CTRL}
567 and SH-SY5Y^{LIN28B} as well as from the pool of 30 embryos using the Qiazol Lysis Reagent
568 (Qiagen), and 10 ng of total RNA solution were reverse transcribed using the miScript II
569 RT Kit (Qiagen). Specific miRNA levels were quantified by qPCR using the TAQMAN
570 microRNA Assay (Life Technologies) for *hsa-miR-let-7a* together with the universal RT

571 primer, according to the manufacturer's protocol. The relative quantities of the miRNAs
572 were calculated using the Cq value after normalization to control the miRNA (*RUN6B*).

573 **Quantification and statistical analysis.** All data were expressed as the mean \pm SEM of
574 experimental triplicates. Statistical significance was determined using the Student's t-test;
575 $p < 0.05$ was considered significant and was marked with an asterisk (*) on the graphs
576 while $p < 0.01$ was marked with two asterisks (**).

577 The statistical significance of the cells' migratory differences related to time-lapse
578 experiments was calculated using the Wilcoxon test (from the R software 'stats' package),
579 and boxplots (using the R software 'stats' package) reported the quartile distribution of
580 related variables.

581

582 **ACKNOWLEDGMENTS**

583 The authors would like to thank the Fondazione Italiana per la Lotta al Neuroblastoma and
584 the Fondazione Veronesi (FUV) for their support. We also thank Elisa Lidron (University of
585 Padua), Valentina Tonelotto (University of Padua), and Claudia Grigoletto (University of
586 Trieste) for their excellent technical assistance.

587

588 **DECLARATION OF INTEREST**

589 The authors declare no potential conflicts of interests.

590

591 **REFERENCES**

592 1. Kerosuo L, Bronner-Fraser M. What is bad in cancer is good in the embryo: Importance
593 of EMT in neural crest development. *Semin Cell Dev Biol* 2012;**3**:320-32.

594

595 2. Anderson DJ, Carnahan JF, Michelsohn A, Patterson PH. Antibody markers identify a
596 common progenitor to sympathetic neurons and chromaffin cells in vivo and reveal the
597 timing of commitment to neuronal differentiation in the sympathoadrenal lineage. *J*
598 *Neurosci* 1991;**11**: 3507–19.

599

- 600 3. Kulesa PM, Gammill LS. Neural crest migration: Patterns, phases and signals. *Dev Biol*
601 2010;**2**:566–8.
- 602
- 603 4. King CE, Wang L, Winograd R, Madison BB, Mongroo PS, Johnstone CN, et al. LIN28B
604 fosters colon cancer migration, invasion and transformation through let-7-dependent and-
605 independent mechanisms. *Oncogene* 2011;**30**:4185–93.
- 606
- 607 5. Xiong H, Zhao W, Wang J, Seifer BJ, Ye C, Chen Y, et al. Oncogenic mechanisms of
608 Lin28 in breast cancer: new functions and therapeutic opportunities. *Oncotarget*
609 2017;**8**:25721–35.
- 610
- 611 6. Hamano R, Miyata H, Yamasaki M, Sugimura K, Tanaka K, Kurokawa Y, et al. High
612 expression of Lin28 is associated with tumour aggressiveness and poor prognosis of
613 patients in oesophagus cancer. *Br J Cancer* 2012;**106**:1415–23.
- 614
- 615 7. Molenaar JJ, Domingo-Fernández R, Ebus ME, Lindner S, Koster J, Drabek K, et al.
616 LIN28B induces NB and enhances MYCN levels via let-7 suppression. *Nat Genet*
617 2012;**44**:1199–206.
- 618
- 619 8. Luksch R, Castellani MR, Collini P, De Bernardi B, Conte M, Gambini C, et al. NB
620 (Peripheral neuroblastic tumours). *Crit Rev Oncol Hematol* 2016;**107**:163–81.
- 621
- 622 9. De Preter K, Vandesompele J, Heimann P, Yigit N, Beckman S, Schramm A, et al.
623 Human fetal neuroblast and NB transcriptome analysis confirms neuroblast origin and
624 highlights NB candidate genes. *Genome Biol* 2006;**7**:R84.
- 625
- 626 10. Shimada H, Ambros IM, Dehner LP, Hata JI, Joshi V V., Roald B, et al. The
627 International NB Pathology Classification (the Shimada system). *Cancer* 1999;**86**:364–72.
- 628

- 629 11. Cohn SL, Pearson ADJ, London WB, Monclair T, Ambros PF, Brodeur GM, et al. The
630 International NB Risk Group (INRG) classification system: An INRG task force report. *J*
631 *Clin Oncol* 2009;**27**:289–97.
- 632
- 633 12. Pugh TJ, Morozova O, Attiyeh EF, Asgharzadeh S, Wei JS, Auclair D, et al. The
634 genetic landscape of high-risk NB. *Nat Genet* 2013;**45**:279–84.
- 635
- 636 13. Moss EG, Lee RC, Ambros V. The cold shock domain protein LIN-28 controls
637 developmental timing in *C. elegans* and is regulated by the *lin-4* RNA. *Cell* 1997;**88**:637–
638 46.
- 639
- 640 14. Tsalikas J, Romer-Seibert J. LIN28: roles and regulation in development and beyond.
641 *Development* 2015;**142**:2397–404.
- 642
- 643 15. Zhou J, Ng SB, Chng WJ. LIN28/LIN28B: An emerging oncogenic driver in cancer
644 stem cells. *Int J Biochem Cell Biol* 2013;**5**:973–8.
- 645
- 646 16. Helsmoortel HH, Bresolin S, Lammens T, Cavé H, Noellke P, Caye A, et al. LIN28B
647 overexpression defines a novel fetal-like subgroup of juvenile myelomonocytic leukemia.
648 *Blood* 2016;**127**:1163–72.
- 649
- 650 17. Guillemot F, Lo LC, Johnson JE, Auerbach A, Anderson DJ, Joyner AL. Mammalian
651 achaete-scute homolog 1 is required for the early development of olfactory and autonomic
652 neurons. *Cell* 1993;**75**:463–76.
- 653
- 654 18. Naef V, Monticelli S, Corsinovi D, Mazzetto MT, Cellerino A, Ori M. The age-regulated
655 zinc finger factor ZNF367 is a new modulator of neuroblast proliferation during embryonic
656 neurogenesis. *Sci Rep* 2018;**8**:11836.
- 657

- 658 19. Stewart RA, Look AT, Kanki JP, Henion PD. Development of the peripheral
659 sympathetic nervous system in zebrafish. *Methods Cell Biol.* 2004;**76**:237–60.
660
- 661 20. Teitelman G, Baker H, Joh TH, Reis DJ. Appearance of catecholamine-synthesizing
662 enzymes during development of rat sympathetic nervous system: Possible role of tissue
663 environment. *Proc Natl Acad Sci U S A* 1979;**76**:509–13.
664
- 665 21. Dutton JR, Antonellis A, Carney TJ, Rodrigues FSLM, Pavan WJ, Ward A, et al. An
666 evolutionarily conserved intronic region controls the spatiotemporal expression of the
667 transcription factor Sox10. *BMC Dev Biol* 2008;**8**:105.
668
- 669 22. Luo R, An M, Arduini BL, Henion PD. Specific pan-neural crest expression of zebrafish
670 crestin throughout embryonic development. *Dev Dyn* 2001;**220**:169–74.
671
- 672 23. Richards M. The Transcriptome Profile of Human Embryonic Stem Cells as Defined by
673 SAGE. *Stem Cells* 2004;**22**:51–64.
674
- 675 24. Kelsh RN, Brand M, Jiang YJ, Heisenberg CP, Lin S, Haffter P, et al. Zebrafish
676 pigmentation mutations and the processes of neural crest development. *Development*
677 1996;**123**:369–89.
678
- 679 25. Theveneau E, Mayor R. Neural crest delamination and migration: From epithelium-to-
680 mesenchyme transition to collective cell migration. *Dev Biol* 2012;**336**:34–54.
681
- 682 26. Heanue TA, Shepherd IT, Burns AJ. Enteric nervous system development in avian and
683 zebrafish models. *Dev Biol* 2016;**417**:129–38.
684
- 685 27. Yu J, Vodyanik MA, Smuga-Otto K, Antosiewicz-Bourget J, Frane JL, Tian S, et al.
686 Induced pluripotent stem cell lines derived from human somatic cells. *Science* 2007;**318**:
687 1917–20.

688

689 28. Mitchison TJ, Cramer LP. Actin-based cell motility and cell locomotion. *Cell*
690 1996;**3**:371–79.

691

692 29. Hood JD, Cheresch DA. Role of integrins in cell invasion and migration. *Nat Rev Cancer*
693 2002;**2**:91–100.

694

695 30. Kragtorp KA, Miller JR. Integrin alpha5 is required for somite rotation and boundary
696 formation in *Xenopus*. *Dev Dyn* 2007;**236**:2713–20.

697

698 31. Julich D, Cobb G, Melo AM, McMillen P, Lawton AK, Mochrie SG, et al. Cross-Scale
699 Integrin Regulation Organizes ECM and Tissue Topology. *Dev Cell* 2015;**34**:33–44.

700

701 32. Banning A, Babuke T, Kurrle N, Meister M, Ruonala M, Tikkanen R. Flotillins regulate
702 focal adhesions by interacting with α -actinin and by influencing the activation of focal
703 adhesion kinase. *Cells* 2018;**7**:E28.

704

705 33. Owens DW, McLean GW, Wyke AW, Paraskeva C, Parkinson EK, Frame MC, et al.
706 The catalytic activity of the Src family kinases is required to disrupt cadherin-dependent
707 cell–cell contacts. *Mol Biol Cell* 2000;**11**: 51–64.

708

709 34. Avizienyte E, Fincham VJ, Brunton VG, Frame MG. Src SH3/2 domain-mediated
710 peripheral accumulation of Src and phospho-myosin is linked to deregulation of E-cadherin
711 and the epithelial–mesenchymal transition. *Mol Biol Cell* 2004;**15**:2794–803.

712

713 35. Wang H, Zhao Q, Deng K, Guo X, Xia J. Lin28: an emerging important oncogene
714 connecting several aspects of cancer. *Tumour Biol* 2016;**37**:2841–8.

715

716 36. Permuth-Wey J, Kim D, Tsai YY, Lin HY, Chen YA, Barnholtz-Sloan J, et al. LIN28B
717 polymorphisms influence susceptibility to epithelial ovarian cancer. *Cancer Res*
718 2011;**71**:3896–903.

719

720 37. Nguyen LH, Robinton DA, Seligson MT, Wu L, Li L, Rakheja D, et al. LIN28B is
721 sufficient to drive liver cancer and necessary for its maintenance in murine models. *Cancer*
722 *Cell* 2014;**26**:248–61.

723

724 38. Zhu S, Lee JS, Guo F, Shin J, Perez-Atayde AR, Kutok JL, et al. Activated ALK
725 Collaborates with MYCN in Neuroblastoma Pathogenesis. *Cancer Cell* 2012;**21**:362–73.

726

727 39. Hennchen M, Stubbusch J, Abarchan-El Makhfi I, Kramer M, Deller T, Pierre-Eugene
728 C, et al. LIN28B and Let-7 in the Control of Sympathetic Neurogenesis and NB
729 Development. *J Neurosci* 2015;**35**:16531–44.

730

731 40. Kalappurakkal JM, Anilkumarr AA, Patra C, van Zanten TS, Sheetz MP, Mayor S.
732 Integrin mechano-chemical signaling generates plasma membrane nanodomains that
733 promote cell spreading. *Cell* 2019;**177**:1738–56.

734

735 41. Laudato S, Patil N, Abba ML, Leupold JH, Benner A, Gaiser T, et al. P53-induced miR-
736 30e-5p inhibits colorectal cancer invasion and metastasis by targeting ITGA6 and ITGB1.
737 *Int J Cancer* 2017;**141**:1879–90.

738

739 42. Brooks DLP, Schwab LP, Krutilina R, Parke DN, Sethuraman A, Hoogewijs D, et al.
740 ITGA6 is directly regulated by hypoxia-inducible factors and enriches for cancer stem cell
741 activity and invasion in metastatic breast cancer models. *Mol Cancer* 2016;**15**:26.

742

743 43. Zhu S, Zhang X, Weichert-Leahey N, Dong Z, Zhang C, Lopez G, et al. LMO1
744 Synergizes with MYCN to Promote NB Initiation and Metastasis. *Cancer Cell*
745 2017;**32**:310–23.

746

747 44. Kim TH, Kim HI, Soung YH, Shaw LA, Chung J. Integrin (alpha6beta4) signals through
748 Src to increase expression of S100A4, a metastasis promoting factor: implications for
749 cancer cell invasion. *Mol Cancer Res* 2009;**7**:1605–12.

750

751 45. Avizienyte E, Frame MC. Src and FAK signalling controls adhesion fate and the
752 epithelial-to-mesenchymal transition. *Curr Opin Cell Biol* 2005;**17**:542–7.

753

754 46. Crawford BD, Henry CA, Clason TA, Becker AL, Hille MB. Activity and distribution of
755 paxillin, focal adhesion kinase, and cadherin indicate cooperative roles
756 during zebrafish morphogenesis. *Mol Biol Cell* 2003;**14**:3065–81.

757

758 47. Bilozur ME, Hay ED. Neural crest migration in 3D extracellular matrix utilizes laminin,
759 fibronectin, or collagen. *Dev Biol* 1988;**125**:19–33.

760

761 48. Westerfield M. *The Zebrafish Book. A Guide for the Laboratory Use of Zebrafish*
762 *(Danio rerio)*, 3rd edn. Univ Oregon Press: Eugene, OR, 1995.

763

764 49. Kimmel CB, Ballard WW, Kimmel SR, Ullmann B, Schilling TF. Stages of embryonic
765 development of the zebrafish. *Dev Dyn* 1995;**203**:253–310.

766

767 50. Kwan KM, Fujimoto E, Grabher C, Mangum BD, Hardy ME, Campbell DS, et al. The
768 Tol2kit: A multisite gateway-based construction Kit for Tol2 transposon transgenesis
769 constructs. *Dev Dyn* 2007;**236**:3088–99.

770

771 51. Holzschuh J, Barrallo-Gimeno A, Ettl AK, Durr K, Knapik EW, Driever W.
772 Noradrenergic neurons in the zebrafish hindbrain are induced by retinoic acid and require
773 tfap2a for expression of the neurotransmitter phenotype. *Development* 2003;**130**:5741–54.

774

- 775 52. Allende ML, Weinberg ES. The expression pattern of two zebrafish achaete-scute
776 homolog (ash) genes is altered in the embryonic brain of the cyclops mutant. *Dev Biol*
777 1994;**166**:509–30.
- 778
- 779 53. Etard C, Gradl D, Kunz M, Eilers M, Wedlich D. Pontin and Reptin regulate cell
780 proliferation in early *Xenopus* embryos in collaboration with c-Myc and Miz-1. *Mech Dev*
781 2005;**122**:545–56.
- 782
- 783 54. Giannetti K, Corsinovi D, Rossino C, Appolloni I, Malatesta P, Ori M. Platelet derived
784 growth factor B gene expression in the *Xenopus laevis* developing central nervous system.
785 *Int J Dev Biol* 2016;**60**:175–9.
- 786
- 787 55. Thisse B, Thisse C. In situ hybridization on whole-mount zebrafish embryos and young
788 larvae. *Methods Mol Biol* 2014;**1211**:53–67.
- 789
- 790 56. Corallo D, Schiavinato A, Trapani V, Moro E, Argenton F, Bonaldo P. Emilin3 is
791 required for notochord sheath integrity and interacts with Scube2 to regulate notochord-
792 derived Hedgehog signals. *Development* 2013;**140**:4594–601.
- 793
- 794 57. Aveic S, Corallo D, Porcù E, Pantile M, Boso D, Zanon C, et al. TP-0903 inhibits
795 neuroblastoma cell growth and enhances the sensitivity to conventional chemotherapy.
796 *Eur J Pharmacol* 2018;**818**:435–48.
- 797
- 798
- 799

1 **FIGURE LEGENDS**

2 **Figure 1. *Lin28b* overexpression causes sympathoadrenal cell loss.** (A) *In situ*
3 hybridization for the progenitor markers *dβh* and *th* in the superior cervical ganglia (dashed
4 squares) of the control (*ctrl*) and *lin28b* embryos at 80 hpf. Scale bar: 100 μm. The fraction
5 of embryos displaying the corresponding phenotype is provided in each panel. (B) The
6 Western blot analysis of the indicated proteins in the control (*ctrl*) and *lin28b* embryos at
7 72 hpf. The molecular weights are indicated in Kilodaltons (KD). Protein quantification is
8 shown in the right panel. The error bars represent SEM. ***p* < 0.01. (C) Labeling of *zash1a*
9 mRNA in 72 hpf control (*ctrl*) and *lin28b* zebrafish embryos. Dashed circles highlight the
10 developing superior cervical ganglia. The fraction of embryos displaying the corresponding
11 phenotype is provided in each panel. (D) The schematic experimental overview is
12 presented on the left side. On the right side, a representative example of a *Xenopus*
13 embryo (out of 76 embryos analyzed) at stage 35 is shown, indicating the expression of
14 the sympathoadrenal marker *reptin* in the developing adrenal medulla (dashed squares).
15 The lateral view of the *lin28b* injected side (right image) and the uninjected side (*ctrl* side,
16 left image) of the same embryo is presented. (E) Proliferation of sympathoadrenal
17 progenitors identified by tyrosine hydroxylase (TH) immunolabeling (red) coupled with EdU
18 incorporation (green) in the control (*ctrl*) and *lin28b* embryos at 80 hpf. The quantification
19 is shown in the right panel (*n* = 30 embryos for each group). *n.s.*: *p* > 0.05. Scale bar: 100
20 μm. (F) The control (*ctrl*) and *lin28b* embryos were stained for activated Caspase-3 (green)
21 and TH (red) to detect apoptosis in the superior cervical ganglia at 80 hpf. Scale bar: 100
22 μm.

23 **Figure 2. *LIN28B*-induced neuroblastoma in zebrafish.** (A) Macroscopic views of the
24 control (*ctrl*) and *hLIN28B* zebrafish at six months of age, showing a tumor mass found in
25 the anterior abdomen (white dashed line). (B) Haematoxylin-Eosin (H&E) staining of the
26 sagittal sections of the tumors in the IRG of six-month-old fish. Scale bar: 100 μm. (C)
27 Immunohistochemical analyses of the sagittal sections of the *Tg(dβh:GFP)* control (*ctrl*)
28 animals and the *hLIN28B* transgenic fish using tyrosine hydroxylase (TH), HuC/D, and
29 Synaptophysin antibodies. Nuclei were counterstained with hematoxylin (purple). Scale
30 bar: 100 μm.

31 **Figure 3. *Lin28b* increased the migration speed of trunk NCC.** (A) Sequential images
32 of a time lapse movie in *Tg(sox10:GFP)* embryos showing the motility of NCC in *lin28b*
33 embryos (white arrows) and controls (*ctrl*). The reported frames were recorded at 19 hpf

34 (T0) after 109 minutes (T109) and 292 minutes (T292). Scale bar: 200 μm . (B) The
35 representative scheme depicting the analysis of zebrafish trunk NCC migration. The
36 migrated distance of NCC (purple) toward the dorsal aorta (dotted line) in the same region
37 of the trunk (from somite 8 to somite 12) of embryos injected with the GFP mRNA (*ctrl*) or
38 with *lin28b* mRNA (*lin28b*) has been analyzed. (C) A total of 50 injected embryos per
39 group were stained with the *crestin* riboprobe at 19 hpf (upper panel) and 24 hpf (lower
40 panel), displaying the migration of trunk NCC toward the ventral region of the notochord
41 (dotted black lines). The quantification of the percentage of the migrated distance is shown
42 in the graph. $*p < 0.05$. Scale bar: 100 μm . (D) The trunk *sox10*⁺ NCC of the uninjected
43 (*ctrl*; left image) and *lin28b* injected (right image) sides of the *Xenopus* analyzed at stage
44 30 (out of 89 embryos analyzed). A migrated distance of NCC (black square brackets)
45 toward the dorsal aorta is depicted. (E) Imaging of the control (*ctrl*) and *lin28b* embryonic
46 pigment patterns at 48 hpf showed melanocytes populating the yolk sac and the equal yolk
47 extension (dashed squares) between the two groups (the average number of melanocytes
48 in controls = 29 ± 4 and *lin28b* embryos = 28 ± 5 , *p-value* = 0.31). (F) The HuC/D antibody
49 staining (green signal) revealed the presence of segmentally arranged dorsal root ganglia
50 in the trunk of both the controls (*ctrl*) and *lin28b* embryos at 4 dpf (the average number of
51 HuC/D⁺ cells in controls = 20 ± 2 and *lin28b* embryos = 22 ± 3 , *p-value* = 0.2). For
52 individual cell counts composing the zebrafish dorsal root ganglia (DRG), the five most
53 caudal DRG labeled with the HuC/D antibody were counted for each condition (*n* = 30
54 embryos per group). (G) The number of HuC/D-positive enteric neurons (green-positive
55 nuclei) remained comparable between the *lin28b* embryos compared to the control (*ctrl*)
56 siblings at 6 dpf (the average number of HuC/D⁺ cells in controls = 36 ± 4 and *lin28b*
57 embryos = 33 ± 5 , *p-value* = 0.4. *n* = 30 embryos per group). Scale bar: 100 μm .

58 **Figure 4. The Overexpression of LIN28B in SH-SY5Y cells potentiates their**
59 **migratory phenotype.** (A) The qPCR analysis showed a significantly increased
60 expression of the stemness markers *Nestin*, *Sox2*, and *Oct4* upon 7 days of *LIN28B*
61 overexpression. The results show the average of three biological replicate experiments.
62 *GAPDH* was used as the internal control. The error bars represent SEM. $**p < 0.01$, $*p <$
63 0.05 . (B) The *let-7a* level was evaluated at several time points upon *LIN28B* induction (48
64 hours [h], 7 days [d], and 14 days) through qPCR analyses. The results display the mean
65 values of the relative expression \pm error bars representing SEM. $**p < 0.01$; *n.s.*: $p > 0.05$.
66 (C) The morphology of the SH-SY5Y^{CTRL} and SH-SY5Y^{LIN28B} cells treated with doxycycline
67 for 7 days (d). Scale bar: 100 μm . (D) Phalloidin (F-Actin) staining (green) of the SH-

68 SY5Y^{CTRL} and SH-SY5Y^{LIN28B} cells upon 0 hours (h) and 7 days (d) of doxycycline
69 treatment. Scale bar: 50 μm . (E) The SH-SY5Y^{CTRL} and SH-SY5Y^{LIN28B} cells were
70 examined for their migratory capacity in a wound healing assay upon 7 days of
71 doxycycline administration. Representative photographs are reported in the left panel. The
72 percentage of wound closure at every time point was calculated relative to the wound
73 width at 0 hours (h, right graph bars). *n.s.*: $p > 0.05$; $**p < 0.01$. Scale bar: 1000 μm . (F)
74 The transwell migration assay on SH-SY5Y^{CTRL} and SH-SY5Y^{LIN28B} cells upon 7 days of
75 doxycycline administration. Migrated cells were stained with DAPI (blue) and cristalviolet
76 (insets) and counted in following for 10 separated fields. $**p < 0.01$. Scale bar: 100 μm .
77 (G) The cell motility tracks of SH-SY5Y^{CTRL} and SH-SY5Y^{LIN28B} cells ($n = 15$ cells tracked)
78 treated with doxycycline for 7 days. The red dots indicate the final cell position on their
79 path. The distances are presented in μm . (H) The dot plot depicting the average cell speed
80 ($\mu\text{m}/\text{min}$) of the SH-SY5Y^{CTRL} and SH-SY5Y^{LIN28B} cells upon 7 days of doxycycline
81 administration. $p = 1.4 \times 10^{-3}$.

82 **Figure 5. LIN28B activates EMT in neuroblastoma cells and increases their invasive**
83 **potential *in vivo*.** (A) The assessment of transwell migration was determined 24 hours
84 after seeding the SH-SY5Y^{CTRL} and SH-SY5Y^{LIN28B} cells pre-treated with doxycycline for 7
85 days. The quantification of migration was determined by measuring the mean fluorescence
86 intensity, and the results are presented on the histogram. $**p < 0.01$. (B) Fluorescent
87 microscopy images of the trunk region of the *Tg(fli1:GFP)* zebrafish embryos with marked
88 vessels (green) injected at 48 hpf with SH-SY5Y^{CTRL} and SH-SY5Y^{LIN28B} cells (red signal)
89 7 days upon treatment with doxycycline. Visualizations of cells at 4 hours post-implantation
90 (hpi) and at 1 day post-implantation (dpi) are depicted. White arrowheads indicate cells
91 disseminated throughout the trunk vasculature. $n =$ number of animals analyzed. Scale
92 bar: 100 μm . (C) The Western blot analysis for the indicated EMT markers on SH-
93 SY5Y^{CTRL} and SH-SY5Y^{LIN28B} upon 7 days of doxycycline. β -Tubulin was used to show
94 equal protein loading. The molecular weights are indicated in Kilodaltons (KD). (D) The
95 overexpression of *LIN28B* for 7 days increased the expression levels of the mesenchymal
96 markers *Twist1*, *Snail*, *N-cadherin*, and *Slug*. *GAPDH* was used as an internal control. $**p$
97 < 0.01 . (E) qPCR analysis for the indicated EMT markers in the ctrl and *lin28b*-
98 overexpressing zebrafish embryos at 48 hpf. The results are normalized to the *gapdh*
99 internal control. The error bars represent SEM. $**$, $p < 0.01$. (F-G) The western blot
100 analysis of 72 hpf (F) and 96 hpf (G) zebrafish embryos extracts for the indicated EMT
101 markers and Lin28b protein. β -Actin was used as a loading control. The molecular weights

102 are indicated in Kilodaltons (KD). The quantification of the same is shown in the right
103 graph bars. * $p < 0.05$; ** $p < 0.01$.

104 **Figure 6. Ectopic expression of *LIN28B* triggers integrin expression and increases**
105 **cell motility potential. (A)** qPCR analysis for *ITGAs* (*ITGA1-6*, 11) and *ITGBs* (*ITGB1*, 4)
106 upon 7 days of *LIN28B* overexpression. *GAPDH* was used as an internal control gene.
107 *n.s.*: * $p < 0.05$; ** $p < 0.01$. **(B)** Immunofluorescence on SH-SY5Y^{CTRL} and SH-SY5Y^{LIN28B}
108 cells upon 7 days of doxycycline administration for ITGA5 (green, upper panel) and ITGA6
109 (lower panel) protein deposition (white arrows). The nuclei were counterstained with DAPI
110 (blue). Scale bar: 50 μm . Insets correspond to higher magnification of the ITGA5/6-positive
111 cells. **(C-D)** The flow cytometry profile of SH-SY5Y^{CTRL} and SH-SY5Y^{LIN28B} cells over 7
112 days of doxycycline administration, showing **(C)** ITGA5-positive (CD49e, $p = 0.05$, left
113 panel) and **(D)** ITGA6-positive (CD49f, right panel, $p = 0.04$) cells. **(E)** The cell motility
114 tracks of SH-SY5Y^{CTRL} and SH-SY5Y^{LIN28B} cells treated with doxycycline for 7 days and
115 incubated with a non-neutralizing IgG control antibody or with the blocking antibody (ab)
116 against ITGA5 (ITGA5ab; 12 cells tracked) prior to the time-lapse imaging. The red dots
117 indicate the final position of the cell migration path. The corresponding average cell
118 speeds of SH-SY5Y^{CTRL} and SH-SY5Y^{LIN28B} are depicted in the box plots. IgG plot: $p = 3.1$
119 $\times 10^{-6}$; ITGA5 plot: $p = 1 \times 10^{-1}$. **(F)** The cell motility tracks of SH-SY5Y^{CTRL} and SH-
120 SY5Y^{LIN28B} cells treated with doxycycline for 7 days and incubated with a non-neutralizing
121 IgG control antibody or the blocking antibody (ab) against ITGA6 (ITGA6ab; 12 cells
122 tracked) prior to the time-lapse imaging. The red dots indicate the final position of the cell
123 migration path. The corresponding average cell speeds of SH-SY5Y^{CTRL} and SH-
124 SY5Y^{LIN28B} are depicted as the box plots. IgG plot: $p = 6 \times 10^{-4}$; ITGA6 plot: $p = 8.9 \times 10^{-1}$.

125 **Figure 7. Ectopic expression of *LIN28B* triggers focal adhesion re-organization and**
126 **activation of integrin/FAK-related signaling pathway.**

127 **(A)** The immunostaining of the focal adhesion (FA) associated adaptor proteins Paxillin,
128 FAK, and Vinculin (green) in combination with Phalloidin (F-Actin, red) is presented. Local
129 redistribution of the proteins in the FAs is indicated by white arrowheads and evidenced
130 as insets. The nuclei were counterstained with DAPI (blue). FAs of 5 cells within 3 random
131 fields were counted, and data were presented as mean \pm SEM from 3 independent
132 experiments. ** $p < 0.01$. **(B)** The Western blot analysis for the indicated markers on SH-
133 SY5Y^{CTRL} and SH-SY5Y^{LIN28B} upon 7 days of doxycycline administration. An antibody
134 against β -Tubulin was used as a loading control. The molecular weights are indicated in
135 Kilodaltons (KD).

136 **Supplemental Figure 1. Generation of a *lin28b*-overexpressing zebrafish model. (A)**
137 Wild-type zebrafish embryos were injected with *lin28b* or GFP mRNA as a control (*ctrl*).
138 The levels of the *lin28b* transcript were assessed by RT-PCR analysis at several time
139 points (18-80 hpf). β -Actin was used as an internal control. The transcript length is
140 indicated as the number of base pairs (bp). An immunoblot (IB) assay was adopted for the
141 analysis of the Lin28b protein levels upon injection at the same time points. β -Actin was
142 used as a loading control. The molecular weight of the proteins was indicated in
143 Kilodaltons (KD). hpf: hours post fertilization. (B) Left panel: images of 48 hpf control (*ctrl*)
144 embryos injected with mCherry mRNA or GFP mRNA. The Brightfield images show no
145 macroscopic alterations after the injection of the control mRNAs. Central panel:
146 representative wild-type uninjected embryo at 48 hpf, showing the absence of endogenous
147 mCherry and GFP fluorescent signals. Right panel: IB assay, followed by a long exposure
148 to detect the wild-type Lin28b protein levels during the indicated developmental stages.
149 The molecular weights are indicated in Kilodaltons (KD). (C) The brightfield images of the
150 control (*ctrl*) and *lin28b* embryos at the indicated developmental stages, showing the
151 absence of visible malformations in the *lin28b*-overexpressing fish and the
152 corresponding *ctrl*. (D) The analysis of *miR-let-7a* mRNA levels at 72 hpf by whole-mount
153 *in situ* hybridization (WISH). *Lin28b* embryos showed a marked loss of staining for *let-7a*
154 when compared to the *ctrl*. The fraction of embryos displaying the corresponding
155 phenotype is provided in each panel. Scale bar: 100 μ m. The qPCR analysis (right panel)
156 showed a significant down-regulation of the *let-7a* transcript in 72 hpf *lin28b* embryos
157 compared to *ctrl*. The error bars represent SEM. **** $p < 0.01$.**

158 **Supplemental Figure 2. *Lin28b* overexpression provokes no apoptosis of**
159 **sympathoadrenal precursors.** Immunofluorescence staining of the superior cervical
160 ganglia (SCG) for the TH sympathoadrenal marker (TH⁺, green) of the 80 hpf control (*ctrl*)
161 and *lin28b* embryos stained with the TUNEL assay for cell death evaluation (red signal).
162 Scale bar: 100 μ m.

163 **Supplemental Figure 3. *Lin28b* does not influence the proliferation or viability of**
164 **NCC. (A)** Cytofluorimetric analysis revealed no significant differences in the percentage
165 (%) of trunk NCC between the *lin28b* -overexpressing and the control (*ctrl*) *Tg(sox10:GFP)*
166 embryos. Uninjected embryos (BLANK) at 19 hpf, 24 hpf, and 28 hpf were used for the
167 flow cytometry parameters set-up. hpf: hours post fertilization; SS: side scatter; *n.s.*: $p >$
168 0.05. (B) Lateral views of the *Tg(sox10:GFP)* control and *lin28b* embryos stained with EdU
169 (green) at 24 hpf. The related quantification of proliferating NCC in three independent

170 experiments is shown in the right panel (data represent means \pm SEM; $n = 30$ embryos for
171 each group). *n.s.*: $p > 0.05$. Scale bar: 100 μm . (C) Lateral views of the trunk NCC
172 (*sox10+*, green) of the control (*ctrl*) and *lin28b* embryos analyzed with the TUNEL assay
173 (red signal) at 24 hpf. The quantification of TUNEL-positive NCC of three independent
174 experiments is shown in the right panel (data are shown as means \pm SEM; $n = 30$ embryos
175 for each group). *n.s.*: $p > 0.05$. Scale bar: 100 μm .

176 **Supplemental Figure 4. Long-term *LIN28B* overexpression enhances the migration**
177 **capability of neuroblastoma cells.** (A) Representative images of clonogenic assays are
178 shown for each cell line. Cells were analyzed for the foci formation during the course of 7
179 and 14 days (d) of doxycycline administration. The number of colonies was calculated by
180 Fiji software (right graphs) after coloration with MTT, and the results are shown as the
181 mean \pm SEM of three independent experiments. *n.s.*: $p > 0.05$. (B) The Western blot
182 analysis in SH-SY5Y^{CTRL} and SH-SY5Y^{LIN28B} cells upon 7 and 14 days (d) of doxycycline
183 administration using the PCNA and GAPDH antibodies as a loading control. The molecular
184 weights are indicated in Kilodaltons (KD). (C) SH-SY5Y^{CTRL} and SH-SY5Y^{LIN28B} cells were
185 treated with doxycycline for 14 days (d), and changes in the cell morphology were
186 observed and photographed by light microscopy. Scale bar: 100 μm . (D) Phalloidin
187 staining (F-Actin) in SH-SY5Y^{CTRL} and SH-SY5Y^{LIN28B} cells upon 14 days (d) of
188 doxycycline treatment revealed a shift in the cell morphology and a reorganization of the
189 stress fibers. Scale bar: 50 μm . (E) The single-cell motility tracks over time (h: hours) of
190 SH-SY5Y^{CTRL} and SH-SY5Y^{LIN28B} after 7 days (d) of doxycyclin induction. Asterisks (white
191 for SH-SY5Y^{CTRL} and yellow for SH-SY5Y^{LIN28B}) indicate the same cell positioning over
192 time. (F) The cell motility tracks of SH-SY5Y^{CTRL} and SH-SY5Y^{LIN28B} cells ($n = 17$ cells
193 tracked) treated with doxycycline for 14 days and captured by time-lapse imaging over a
194 12-hour period at 10 minute intervals using the Image J "manual tracking" plug in. The red
195 dots indicate the final position of the cells during their migration path. (G) The dot plot
196 depicting the average cell speed ($\mu\text{m}/\text{min}$) of SH-SY5Y^{CTRL} and SH-SY5Y^{LIN28B} cells upon
197 14 days of doxycycline administration. The data are representative of three experiments.
198 The error bars indicate SEM. $p = 1.5 \times 10^{-5}$. (H) The single-cell motility tracks over time of
199 SH-SY5Y^{CTRL} and SH-SY5Y^{LIN28B} after 14 days (d) of doxycyclin induction. The asterisks
200 (white for SH-SY5Y^{CTRL} and yellow for SH-SY5Y^{LIN28B}) indicate the same cell positioning
201 over time.

202 **Supplemental Figure 5. Prolonged *LIN28B* overexpression triggers EMT.** (A) The
203 Western blot analysis showing the mesenchymal markers Twist1, Vimentin, Snail, and N-

204 cadherin and the epithelial E-cadherin after 14 days of *LIN28B* overexpression. GAPDH
205 was used to show equal protein loading. The molecular weights are indicated in
206 Kilodaltons (KD). **(B)** Immunofluorescence of the SH-SY5Y^{CTRL} and SH-SY5Y^{LIN28B} cells
207 over 14 days of doxycycline administration showed the induction of ITGA5 protein (green,
208 upper panel) and ITGA6 (green, lower panel) in the SH-SY5Y^{LIN28B} cells (white arrows).
209 Nuclei were counterstained with DAPI (blue). Scale bar: 50 μ m. **(C-D)**
210 Immunofluorescence analysis of the SH-SY5Y^{CTRL} and SH-SY5Y^{LIN28B} cells over **(C)** 7
211 days (d) and **(D)** 14 days (d) of doxycycline administration, labeled with the ITGA5
212 antibody (green, upper panel) and ITGA6 (green, lower panel) without the membrane
213 permeabilization. The staining with only secondary antibodies was used as a negative
214 control (negative ctrl). The nuclei were labeled with Hoechst (blue). White arrows point out
215 the integrin protein accumulation. Scale bar: 50 μ m.

216 **Supplemental Figure 6. Long-term *LIN28B* overexpression stimulates focal adhesion**
217 **creation. (A)** Confocal immunofluorescence images of SH-SY5Y^{CTRL} and SH-SY5Y^{LIN28B}
218 stained with antibodies against Paxillin, FAK, and Vinculin (green) after 14 days of
219 doxycyclin administration. F-Actin filaments were labeled with phalloidin (F-Actin; red), and
220 the nuclei were counterstained with DAPI (blue). Scale bar: 20 μ m. Statistical analysis of
221 the number of focal adhesions (FAs) per cell is presented. FAs of five cells of three
222 random fields were counted. Columns represent the means from three independent
223 experiments, and the bars represent the SEM. $**p < 0.01$. **(B)** The Western blot analysis
224 for the indicated markers on SH-SY5Y^{CTRL} and SH-SY5Y^{LIN28B} upon 7 days of doxycycline
225 induction. β -Tubulin was used as a loading control. The molecular weights are indicated in
226 Kilodaltons (KD). **(C)** The Western blot analysis for the indicated markers on SH-SY5Y^{CTRL}
227 and SH-SY5Y^{LIN28B} upon 14 days of doxycycline induction. β -Tubulin was used as a
228 loading control. The molecular weights are indicated in Kilodaltons (KD).

229 **Supplemental Video S1. Related to Figure 3. *LIN28B* increased the migration of**
230 **trunk neural crest cells (NCC).** *Tg(sox10:GFP)* embryos were injected with **(A)** mCherry
231 (ctrl) or **(B)** *lin28b* mRNA and time lapse on trunk NCC was performed on 19 hpf embryos
232 for eight hours.

233 **Supplemental Video S2. Related to Figure 4. Overexpression of *LIN28B* in SH-SY5Y**
234 **cells affects their pro-migratory potential.** Time-lapse video of **(A)** SH-SY5Y^{CTRL} and
235 **(B)** SH-SY5Y^{LIN28B} cells treated with doxycycline for 7 days and seeded into a plastic
236 chamber. Frames were captured over a 12-hour period at 10 min intervals.

237 **Supplemental Video S3. Related to Supplemental Figure 4. Overexpression of**
238 ***LIN28B* in SH-SY5Y cells affects their pro-migratory potential.** Time-lapse video of (A)
239 SH-SY5Y^{CTRL} and (B) SH-SY5Y^{LIN28B} cells treated with doxycycline for 14 days and
240 seeded into a plastic chamber. Frames were captured over a 12-hours period at 10 min
241 intervals.

242 **Supplemental Video S4. Related to Figure 6. Overexpression of *LIN28B* in SH-SY5Y**
243 **cells affects their pro-migratory potential.** Time-lapse video of (A) SH-SY5Y^{CTRL} and
244 (B) SH-SY5Y^{LIN28B} cells pre-treated with doxycycline for 7 days and followed by treatment
245 with 10 µg/ml of IgG negative control antibody for 30 minutes. Frames were captured over
246 a 12-hour period at 10 min intervals.

247 **Supplemental Video S5. Related to Figure 6. Pro-migratory potential of *LIN28B***
248 **overexpressing SH-SY5Y cells in impaired upon ITGA6 block.** Time-lapse video of (A)
249 SH-SY5Y^{CTRL} and (B) SH-SY5Y^{LIN28B} cells pre-treated with doxycycline for 7 days followed
250 by 30 minutes treatment with 10 µg/ml of ITGA6 blocking antibody. Frames were captured
251 over a 12-hour period at 10 min intervals.

252 **Supplemental Video S6. Related to Figure 6. Overexpression of *LIN28B* in SH-SY5Y**
253 **cells affects their malignant phenotype.** Time-lapse video of (A) SH-SY5Y^{CTRL} (B) and
254 SH-SY5Y^{LIN28B} cells pre-treated with doxycycline for 7 days followed by 30 minutes
255 treatment with 10 µg/ml of IgG negative control antibody. Frames were captured over a 12-
256 hour period at 10 min intervals.

257 **Supplemental Video S7. Related to Figure 6. Pro-migratory potential of *LIN28B***
258 **overexpressing SH-SY5Y cells in impaired upon ITGA5 block.** Time-lapse video of (A)
259 SH-SY5Y^{CTRL} (B) and SH-SY5Y^{LIN28B} cells pre-treated with doxycycline for 7 days followed
260 by 30 minutes treatment with 10 µg/ml of ITGA5 blocking antibody. Frames were captured
261 over a 12-hour period at 10 min intervals.

262 **Supplemental Table S1.** List of primary and secondary antibodies used for
263 immunofluorescence and western blotting studies.

264 **Supplemental Table S2.** List of primers used for RT-PCR and qPCR studies.

265

266

Figure 1

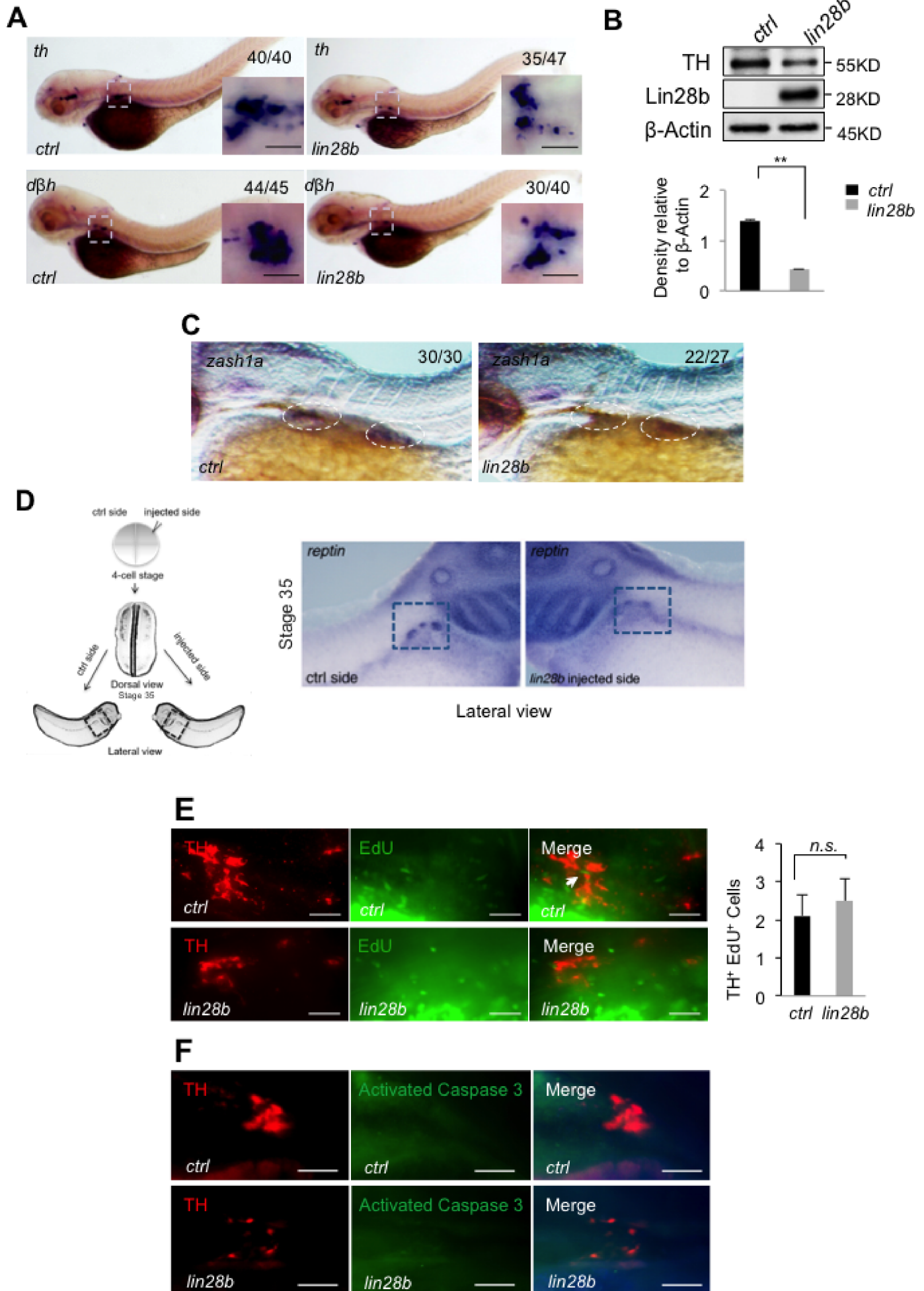


Figure 2

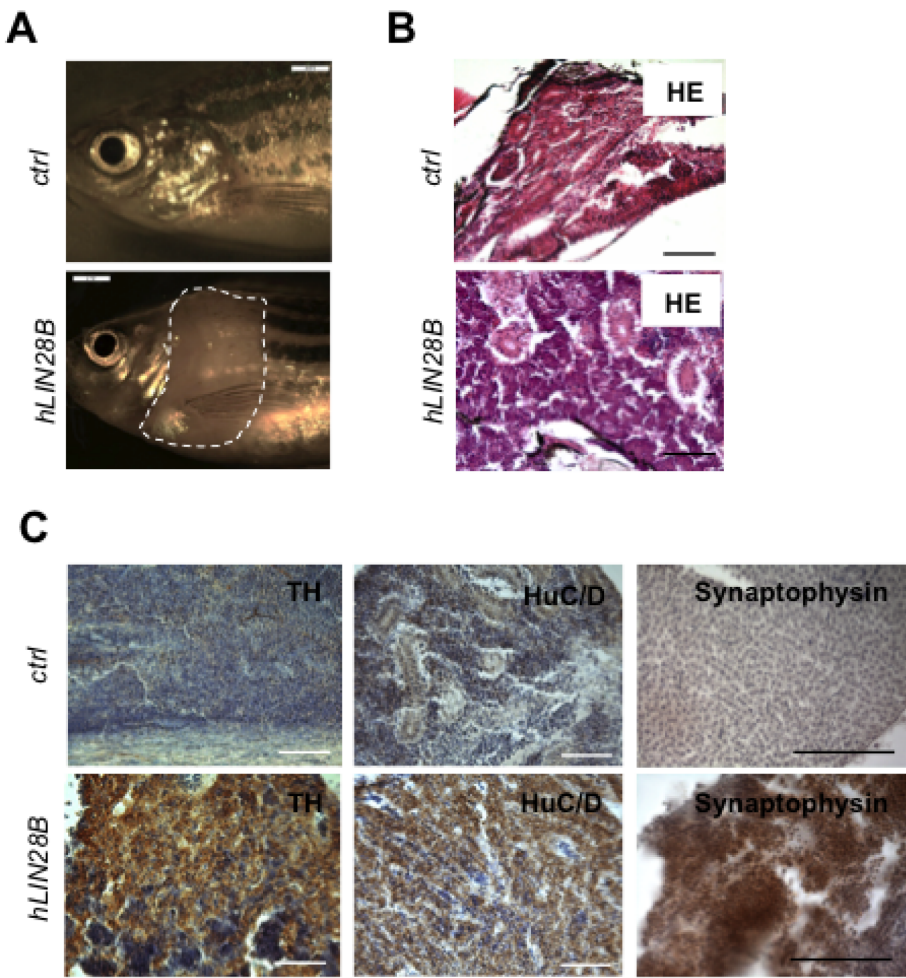


Figure 3

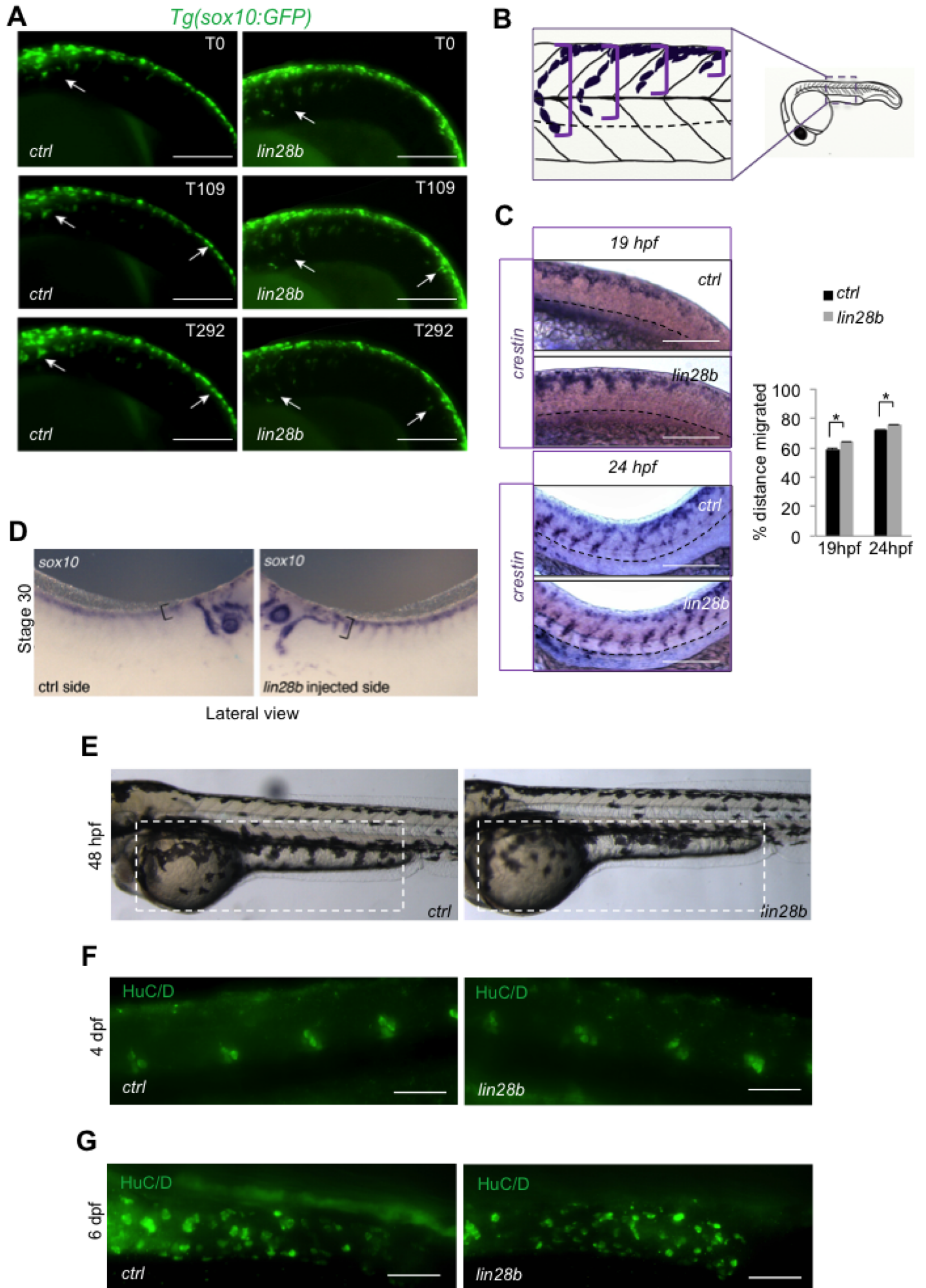


Figure 4

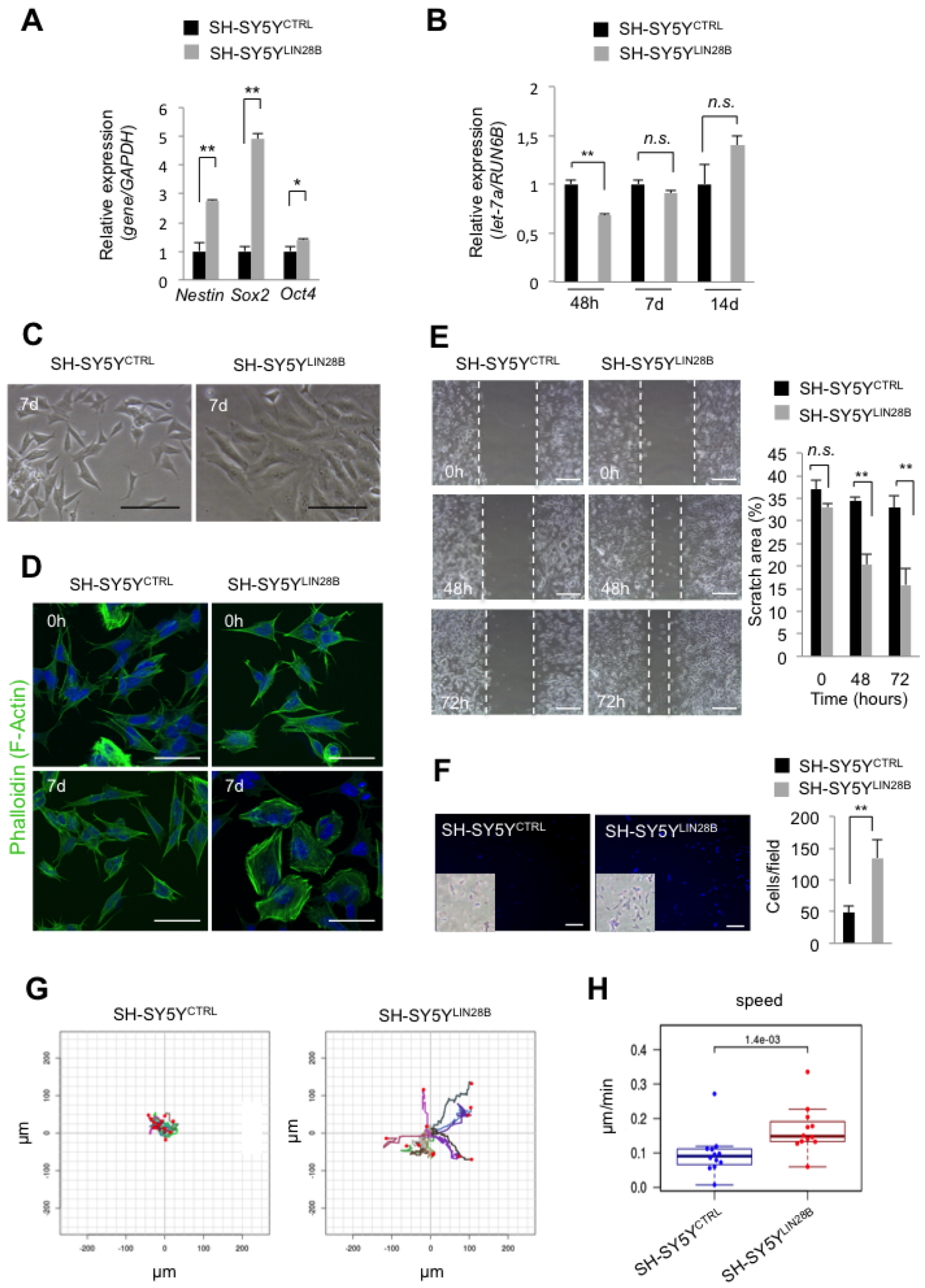


Figure 5

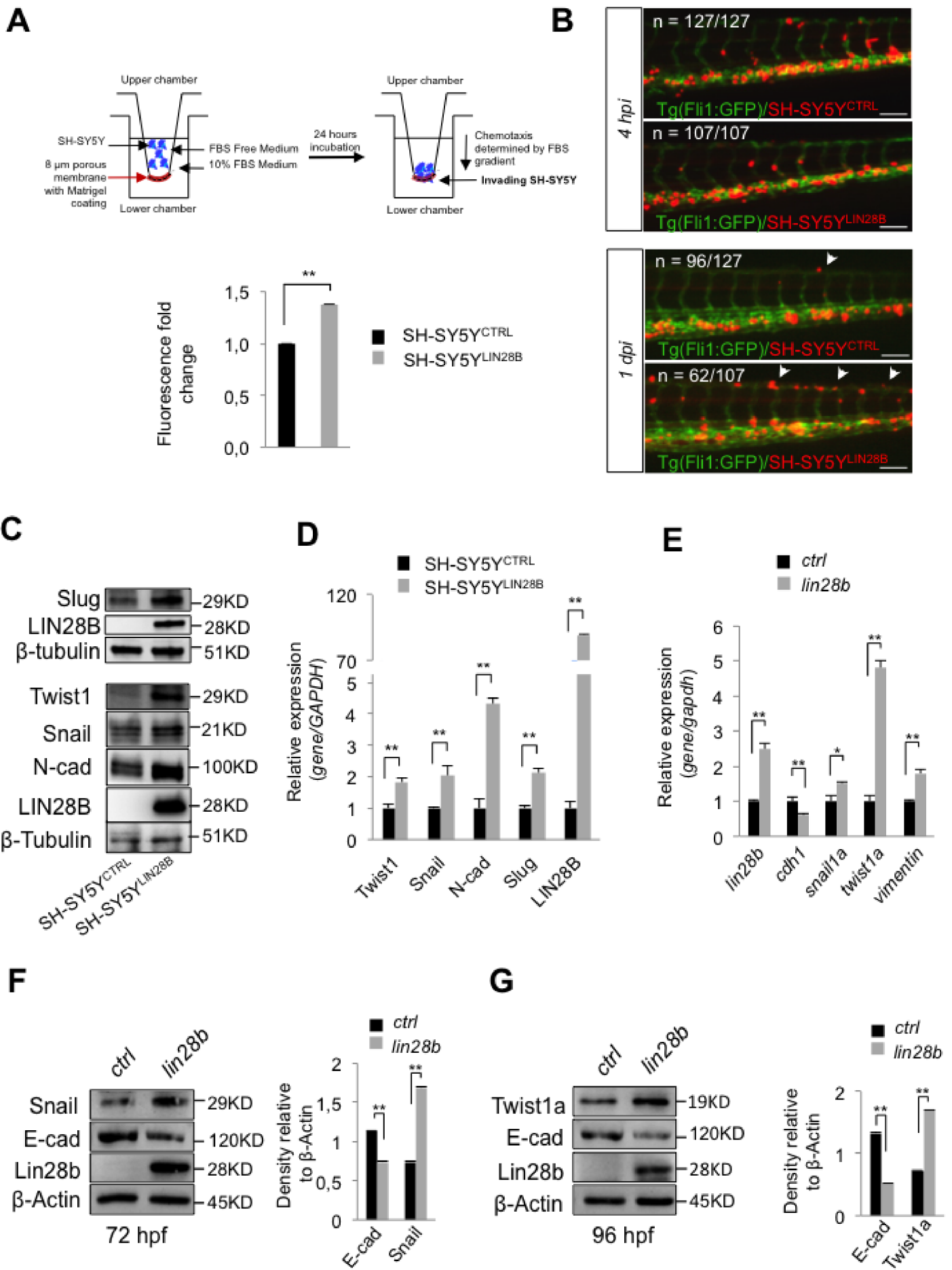


Figure 6

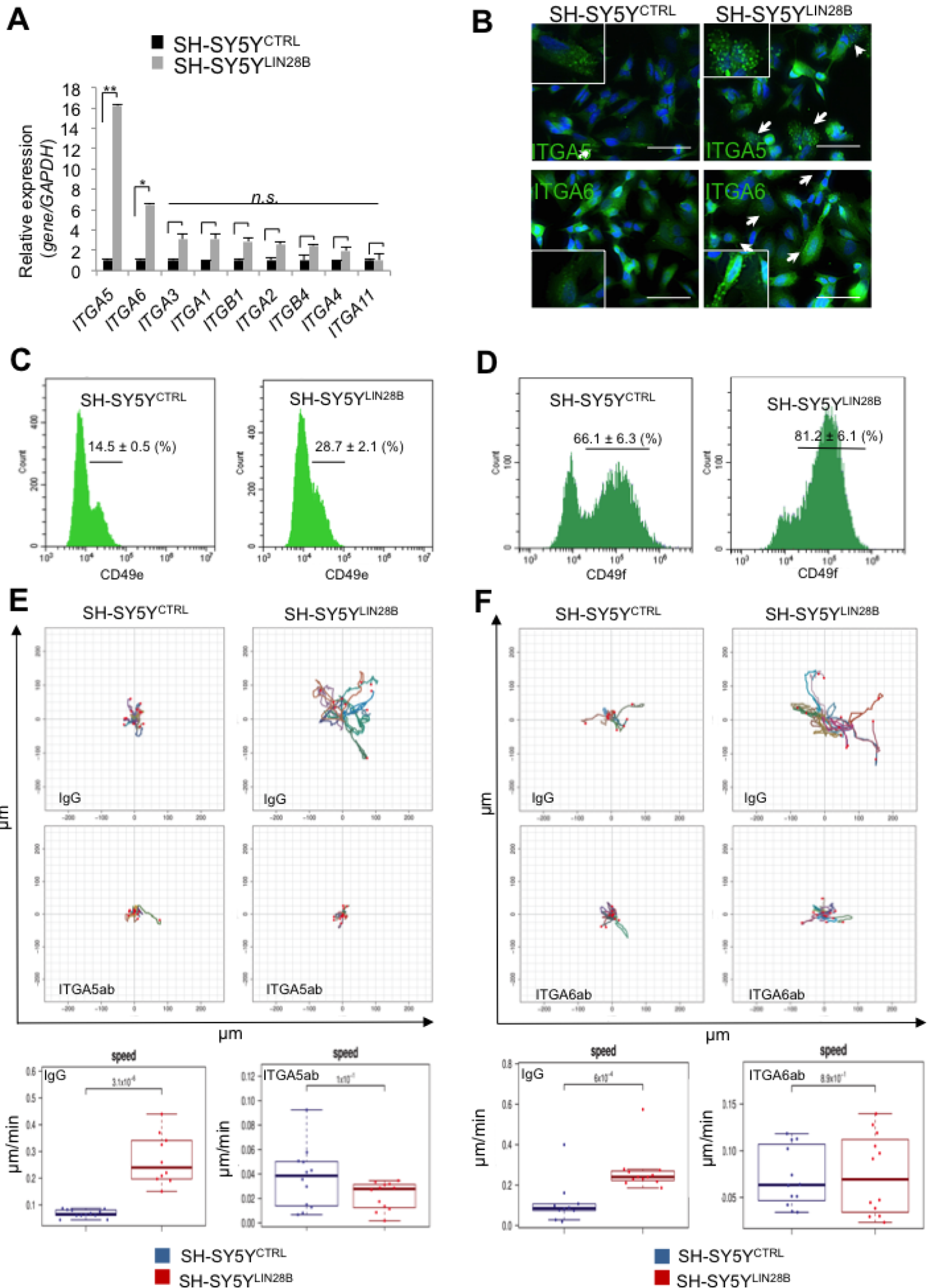


Figure 7

